УДК 553.067 DOI 10.31242/2618-9712-2021-26-2-3

Mineralization in the Kildyam mafic volcanic rocks – a magmatic contribution to ore-forming fluids (Central Yakutia, Russia)

A.V. Kostin

Diamond and Precious Metal Geology Institute, SB RAS, Yakutsk, Russia a.v.kostin2006@rambler.ru

Аннотация. Mineral assemblages and processes occurring in olivine-pyroxenites, andesite, and dacite volcanic settings of the Kildyam Late Jurassic complex in Central Yakutia are investigated. The methods involved in the study include detailed sensing and mapping using ESRI ArcGis. Imagery Service, field observations, minerals and glass identification, recognition of vesicle composition. The results obtained in the study support the igneous vapor transport of ore elements in the andesitic system and imply preconcentration of iron, copper and \pm gold and silver during lava solidification into magnetite rich lava flows. The major components of the Kildyam andesite alloys are Fe, Cu, Sn, Pb, Zn, and Ag. Alloy element maps show a covariance of Cu±(Zn, Sn, Ni, Fe), and Ag concentrations varied independently. This research confirmed that tholeitic trend of iron-rich olivine-pyroxenites evolve towards two immiscible liquids: (1) magnetite lava, and (2) melilitite matrix. Further evolution leads to the separation of native iron and the transition of lavas to the calc-alkaline trend. Petrographic and microprobe studies confirmed the liquid immiscibility in silicate melts during crystallization. Immiscible liquids are preserved as globules of one glass in another in andesites and as melted inclusions of native iron in the matrix, clinopyroxene and plagioclase phenocrysts. The vesiclehosted alloys and sulfides provide significant new data on metal transportation and precipitation from hightemperature magmatic vapors. During syneruptive vapor phase exsolution, volatile metals (Cu–Zn, Fe–Al– Cu, Ni–Fe–Cu–Sn) and Ag–Cu sulfides contribute to the formation of economic concentrations.

Keywords: Kildyam volcanic complex, liquid immiscibility, metallic alloys, melilitic and magnetite lavas, copper, silver.

Introduction

Volcanic eruptions thought to be a viable process for the accumulation of metals at or near the surface and may have a great role in metallogenesis. It is well known, that mafic magma was fundamental in delivering sulfur and chalcophile elements to overlying felsic magma chambers and could contribute to the formation of many economic deposits. This model is described in details for Mount Pinatubo in the Philippines and Bingham Canyon, Utah, site of the largest copper and gold deposit in North America [1].

Ore minerals preserved in volcanic rocks can be used to trace element evolution in magmatic systems and to confirm the potential magmatic contribution to ore-forming fluids. There is no doubt that list of metals in vesicle walls of volcanic lava indicates the ore forming process with base (Fe, Cu, Pb, Zn, Sn) and precious (Au, Ag, PGM) metals complex. The list of metals may differ in mafic and felsic volcanism.

Many volcano researchers point out that volcanic eruptions and open-system degassing contribute

large quantities of metals into the host environment. The crystalline particles of gold has been documented in the plume near the crater from Mount Erebus, Antarctica [2]. Kilauea volcano produced a large suite of metals (Pb, Cd, Cu, Zn and several others) and sulfur over an extended period of time [3]. Similar behavior of Stromboli volcano during degassing of its S-Cl-rich shoshonitic magma brought high enrichment with the S, Se, Br, Cl, Cd, Bi, In, As, Sb, Sn, F, Au, Pb, Cr, Cu derived from volcanic ash [4]. Latest research [5] describe metallic alloys in vesicles of mafic scoria and lava erupted from volcanoes in Hawaii and Italy. Li P. and Boudreau A.E. documented the rare occurrence of native Cu-Au-Ag alloys and the large native Au and Ag grain size in lava flows from Kīlauea and Mauna Loa volcanoes (Hawaii), and a mid-oceanic-ridge basalt (MORB) and suggested separate metal precipitation mechanisms [6]. As an example of Mt. St. Helens Most it was proved that the trace elements in the gases are volatilized from shallow magma as simple chlorides and near-surface cooling of the gases trig-

© Kostin A.V., 2021 49

gers precipitation of oxides, sulfides, halides, tungstates, and native elements [7]. The Tolbachik eruptions in Kamchatka produced Cu-rich magnesioferrite in association with hematite, tenorite, halite, sylvite, and Ca-rich silicates esseneite and Na-rich melilite [8]. It is assumed that a combination of gasrock interaction was responsible for extraction of metals from the basaltic wall rocks and deposition of Cu-, Fe- and Cu-Fe-oxides and native gold [9]. Ovalle J.T., La Cruz N.L., Reich M. et al. believe that El Laco iron deposit in the Central Andes, and similar deposits worldwide, were formed by a synergistic combination of common magmatic processes enhanced during the evolution of caldera-related explosive volcanic systems [10].

Kildyam Mesozoic eruptions in Central Yakutia with iron oxide mineralization has been interpreted as lava flows and feeder dykes, formed from ironrich pyroxenite magma as a result of liquid immiscibility [11]. Mineralization is associated with andesitic lavas and occur as massive, tabular and stratified bodies, and pyroclastic ores. Our research confirmed that tholeiitic trend of iron-rich pyroxenites evolves towards two immiscible liquids - magnetite lava and melilitite matrix. Further evolution leads to the separation of native iron and the transition of lavas to the calc-alkaline trend. Petrographic and microprobe studies confirmed the liquid immiscibility in silicate melts during crystallization. Immiscible liquids are preserved as globules of one glass in another in andesites and as melted inclusions of native iron in matrix, clinopyroxene and plagioclase phenocrysts.

Segregation of immiscible iron and sulphide melts from ultramafic and mafic magmas are of economic importance for some elements. Immiscibility of iron- and silica-rich melts during andesitic volcanism led to the formation of exotic varieties of magnetite-rich volcanic rocks. Segregation have many common features with the Kiruna type Pliocene El Laco volcano hosted iron oxide deposit.

Materials and Methods

Earlier rocks and sulfides assemblages were characterized throughout the Kildyam Volcanic Complex (Kangalassky terrace at the left bank of the Lena River, 26 km north of Yakutsk) to better understand oxide/sulfide saturation balance [11]. The following methods for this research include a sequence of geological and mineralogical settings.

First, detail sensing and mapping of the Upper Jurassic volcanic successions, using SAS.Planet free application to view and download satellite maps submitted by ESRI ArcGis.Imagery Service. Based on the detalization level from z12 to z18, it become possible to upload high-resolution images into the spatial chain, showing image refinement in progress. The water shade map enhances visualization perceptions of ArcGis Imagery. The samples used in this study are from precisely known geographic location and geological environment. Our spatial detail investigation reveal that lava units are 10–25 m thick and covering more than 100 sq. km, and include at least three discovered volcanic centers in surrounding of the Upper Jurassic sediments. The main structures are feeder dykes, lava flows and cones within red tuffs, extrusions and subvolcanic linear bodies Figure 1.

Second, all styles of field surface samples classified as volcanic, sedimentary or ore, cut with a circular saw and representative pieces added to the collection. The remaining part of each sample used to prepare polished sections for preliminary mineral identification with polarized light microscopy. Major minerals in lavas and sediments determined by x-ray phase analysis using D2 PHASER diffractometer. Obviously, along the path of the movement, lava contaminate fragments of different host rocks and carry xenoliths and phenocryst from different stratigraphic horizons, so usually the bulk chemical analyses of volcanic rocks are not representative. All quantitative microprobe analysis of lava glass include areal and spot analyses. Backscattered electron (BSE) images supply all analyses with detailed mapping data on the chemistry of the volcanic glass variety. Phenocryst, scoria and preserved vesicles excluded from the investigated lava samples to obtain a pure composition of the lava Figure 2. All microprobe and x-ray analyses carried in the Diamond and Precious Metal Geology Institute, Siberian Branch, Russian Academy of Sciences (DPMGI SB RAS). Minerals and glass identified with scanning electron microscope JSM-6480LV with energy spectrometer INCA-Energy, with 20 kV of accelerating voltage at the cathode. Samples were prepared from polished sections with a sprayed thin conductive layer of carbon.

Third, phenocrysts considered as the evidence of a long-time forming magmatic structure during the Kildyam volcanic history. Numerous euhedral forms with zoning and late dissolving are typical structures among Kildyam phenocrysts, and originally brought from the different depth levels. Both of the phenocrysts styles are of the different nature than the host lava Figure 3. Iron-rich clinopyroxene zones

MINERALIZATION IN THE KILDYAM MAFIC VOLCANIC ROCKS

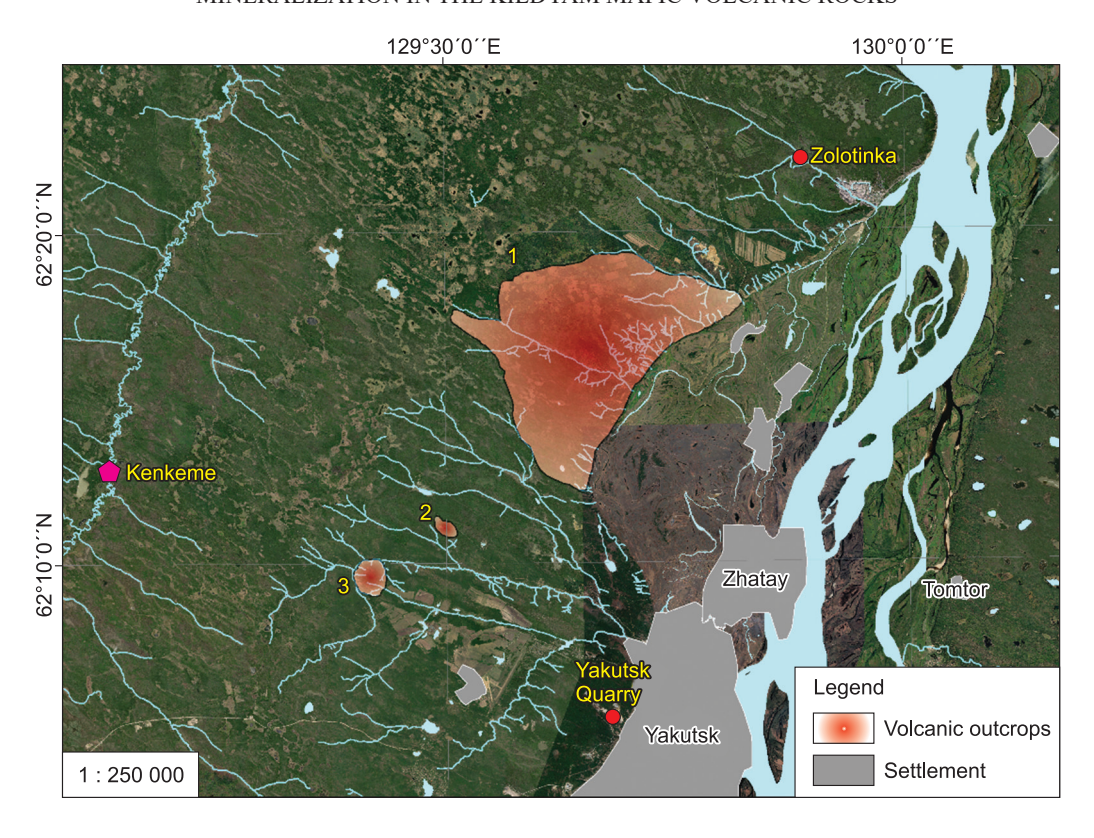


Fig. 1. Kildyam volcanic settings, located near the city of Yakutsk and nearby placer pyrope after Afanasiev et al. [12] and gold manifestations after Smelov and Surnin [13].

Volcanic outcrops: 1 – Main Kildyam volcanic field with subvolcanic and volcanic (102.9 sq km) succession; 2 – Feeder dykes with lava flows (1.0 sq km); 3 – Volcanic cone structure (3.1 sq km). The watershed map (yellow) enhances visualization perceptions of geological structures in ArcGis Imagery; grey areas show settlement locations.

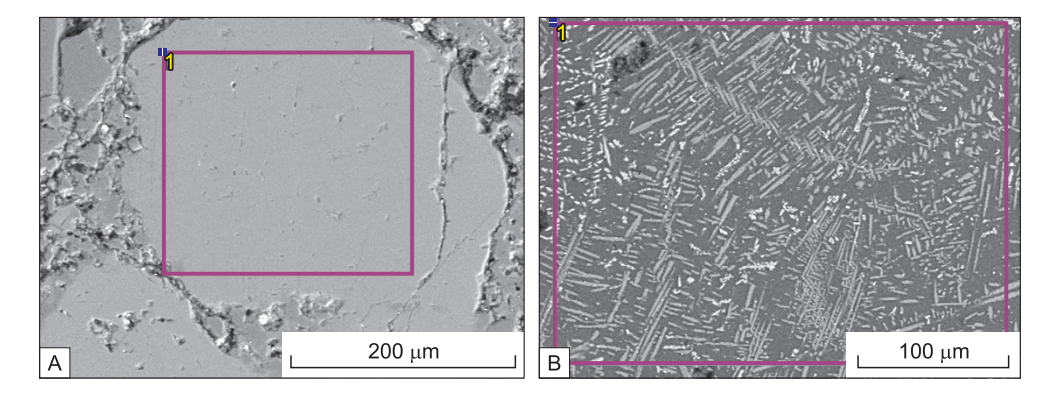


Fig. 2. BSE images of homogeneous lava glass and dendritic skeletal crystals in lava glass.

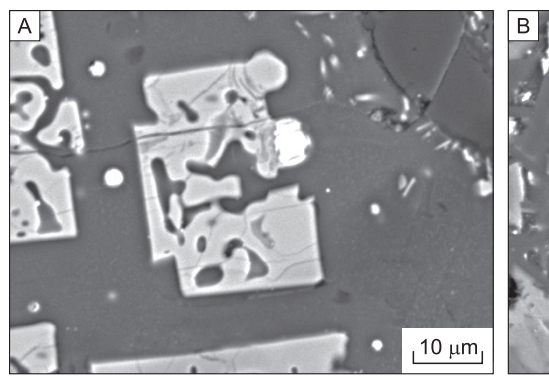
look brighter in backscattered electron (BSE) imagery and show progress in iron saturation from the center to the edge of the crystals. Olivine dissolving structures evidences to a long time migration history.

Fourth, our findings provide a new evidence for high concentration of cristobalite. Volatiles include cristobalite with trace quantities of Ag, Cu, and K–Fe sulphides, Cu–Zn, Fe–Al–Cu, and Ni-Fe-Cu-Sn alloys, and halite. Vesicles within the volcanic products

of Kildyam imaged as optical photographs and backscattered electron images. Native metals with large atomic weights like Ag and Cu recognized by their brightness in backscattered electron (BSE) imagery.

Results

Kildyam is a Late Jurassic volcanic complex in the transition zone between the Siberian platform and the Verkhoyansk-Kolyma folded region in Cen-



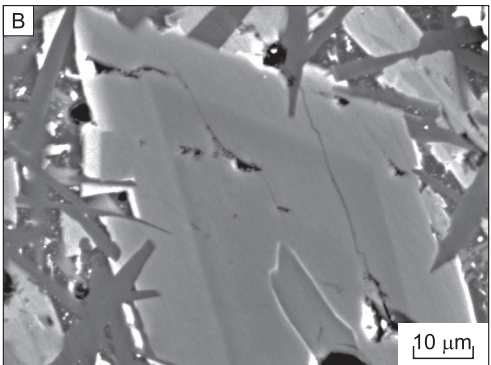


Fig. 3. Phenocrysts in andesitic lava. A – Olivine (average $Fo_{0.105}Fa_{0.895}$); B – Clinopyroxene zoning crystals.

tral Yakutia [14, 15]. The Kildyam volcanic field covers totally 106 km². It consists of several small eruptive centers with a conical morphology and fissure outpourings of lavas. The main varieties of volcanic rocks include volcanic tuff, pumice, lava, lavabreccia, ignimbrites of dacite series, lava and lavabreccia of andesite series, subvolcanic pyroxenite and magnetite lava. We focus on three specific observations of the Kildyam, Namtsyr and Markhinka volcanic outcrops (Table 1).

1. Rocks – general character and distribution

Initially Kildyam outcrops were mapped using an easily identified red tuff units [16], which were traced extensively using SAT images from ArcGIS Earth 1.10.1 free software tool [17, 18]. Outcrops of red tuffs and lavas found in several disparate locations, each with different rock styles and characteristics. Interpretation and selective ground reconnaissance allowed correlating rock similarities between outcrops into one clinopyroxenite-andesite-dacite

volcanic succession. The investigated lava samples, scoria and preserved vesicles represent at least three different faces styles, based on the lava textures and associated major element distribution.

Kildyam volcanic rocks classified into three subtypes according to their SiO₂ content, relation to the surface and stratigraphic distribution of units. Lava analyses introduce three group of volcanic rocks – olivine-clinopyroxenite (1), silica and orthoclase mineral glass, andesite-basalt, andesite, trachyandesite, trachyte-trachydacite and melilitite (2) and rhyodacite (3). Initially two factors have an impact on rocks general characteristics and distribution; (1) porosity is highly variable in different facies of the Kildyam lava flow; (2) volatiles have a substantial influence on the petrogenesis processes, e.g. the formation of economic ore deposit.

Olivine-clinopyroxenite. Subvolcanic complex is comprised of a brecciated linear body, fine grained (at 95 m elevation) to partially melted (at 184 m el-

Table 1

Locations and descriptions of the key outcrops in Kildvam lava

Locations and descriptions of the key outerops in Kndyam fava										
Locality	Coordinates (dd°mm'ss.s")	Elevation (m)	Description							
29 km North from Yakutsk, and 3.5 km West from Kildyam village	62.27425N 129.71313E	160	Kildyam group of small open pits with red tuff, mined before 1970 for the roads construction purpose. Lava lying below is not mined and represent a good ground for study. A numerous Late Jurassic flora fossils were collected							
13.5 km North-West from Yakutsk towards Namtsyr road direction	62.18543N 129.493888E	198	Namtsyr open pit exposed a full section from Late Jurassic sandstone, lava, red tuff with flora fossils, coal and sand							
A temporary 8.5 km summer road, North-West from Magan airstrip	62.158337N 129.41908E	225	Markhinka Ring is a new undiscovered volcanic structure. River sections exposing cliffs from the river bed to the top of the annular volcanic plateau							

evation) olivine-clinopyroxenite clearly show gradual transition to molten rocks. Olivine-clinopyroxenite comprises a lower zone breccia body of finegrained subvolcanic rock, cemented with dacite lava and pumice (samples 1039 and 1051 SiO_2 – 41.17–37.44, TiO_2 – 0.88–0.81, $\mathrm{Al_2O_3}$ – 9.31–11.76, $\mathrm{Fe_2O_3}$ – 15.02–7.35, FeO – 16.3–26.78, MnO – 1.51–2.21, MgO – 1.63–1.19, CaO – 12.03–9.56, $\mathrm{Na_2O}$ – 0.21–0.26, $\mathrm{K_2O}$ – 0.11–0.12, $\mathrm{P_2O_5}$ – 0.07–0, $\mathrm{H_2O^+}$ – 0.67–0.73, $\mathrm{H_2O^-}$ – 0.54-0.5, $\mathrm{CO_2}$ – 0-0.07, S – 0.47-0.75, LOI – 0.69-0.91). In general parental magma indicating srtong incorporation of Fe into mafic silicates (augite and fayalite).

At an altitude of 95 m (Figure 4B) it is a heavy and dense (3.41 g / cm³) fine-grained dark-green rock of allotriomorphic and rarely panidiomorphic structure. The rock contains 48.1 % of pyroxene (augite, rarely hedenbergite), 23.6 % of plagioclase (bitownite-anorthite), 16.8 % of olivine (average Fo_{0.105}Fa_{0.895}), 6.07 % of magnetite, 1.79 % of calcite and 0.75 % of troilite. Less common minerals are Ba-feldspar celsian and K-Ba-feldspar hyalophane. At an altitude of 184 m prevail (Figure 4C) multistage carapace lavas with down-flow textural modifications: (a) flow fold; (b) lava layer shift; (c) degassing channel.

Ore minerals are concentrated as globules of troilite and magnetite in equal proportions and surrounded with olivine rims. Olivine-pyroxenite ore mineral assemblage is composed of elongated shape globules of troilite and magnetite. Ore globules have a circular cross-section in one direction (up to 0.7 cm in size), and are elongated several times in the other Figure 5.

Anomalously high Fe/S ratios in ore globules attributed to initial anomalous Fe/S ratios in the Kildyam parental magma source, early shallow-level degassing and late S loss to hydrothermal fluids. Data obtained from Kildyam can be evaluated with the current models for sulphur saturation in ironrich mafic magmas to estimate initial sulfur concentrations, degree of fractionation, composition of sulfide liquids and degree of post-magmatic sulfur loss [6, 19].

Andesitic lavas. The outcrops showing that andesitic lavas first penetrate as feeder dikes through Late Jurassic sandstones (3.0 m) along a fissure conduit and then cover the sandstones with 2–5 m layer. Lava flow covered with a layer of crystalloclastic tuffs, about 1.5 m thick, and brecciated by the next andesite lava flows.

Andesites and andesibasalts are massive and amygdaloid, porphyry or oligophyry, interspersed

with polysynthetically twinned plagioclase in the pilotaxite or intersertal bulk, were thin andesine leysts and clinopyroxene microprisms are lockated in the background of decomposed, intensely chloritized and oxidized glass. Variolitic andesibasalts are finely bubbled, composed of radiant and radially radiant accretions of needle-like crystals of clinopyroxene and labrador, in the brown decomposed glass. They contain inclusions of black graphitized coal up to 2–2.5 mm in size with no signs of burning. The brand of the lamellae of clinopyroxene and plagioclase in contact with coal wrap around these inclusions.

Lavabreccias represented by various-sized fragments of hyalopilite andesites or variolitic andesibsalts in bubble glass of hyaline structure of daciterhyodacite composition, containing the smallest microliths, comminuted grains and feldspar crystallites. Clastolava include large pyroxenite xenoliths, were grains of partially uralized clinopyroxene germinate with andesite plagioclase leists. Presumably, such accumulations can be carried out during the outpouring of lava basement fragments Figure 6.

Andesitic lava from a middle zone has a density of 2.88–2.92 g / cm³. Samples 1030/4A and 1030/8 show the bulk of $SiO_2 - 56.02-56.38$, $TiO_2 - 0.69-$ 0.16, $Al_2O_3 - 13.45-12.98$, $Fe_2O_3 - 1.57-0.65$, FeO - 7.2-4.93, MnO - 0.35-0.3, MgO - 2.03-2.62, CaO – 12.12–16.32, Na₂O – 1.9–2.16, K₂O – 2.05-2.05, $P_2O_5 - 0.14-0.07$, $H_2O^+ - 0.39-0.46$, $H_2O^- - 0.48 - 0.14$, $CO_2 - 0.27 - 0.2$, S - 0.35 - 0.3, LOI - 0.8-0.07. The Pt content of 0.11 g/t determined by the ICP-MS method. CIPW normative mineral calculation show (in %): quartz 7.29–12.32, plagioclase 37.94-38.19, orthoclase 12.11, diopside 28.43–29.83, wollastonite 0.06-10.6, ilmenite 0.3– 1.31, magnetite 0.94-2.28, apatite 0.1600.32, pyrite 0.64-0.74, calcite 0.45-0.61. Immiscibility of ironand silica-rich melts during andesitic volcanism led to the formation of exotic varieties of magnetite-rich volcanic rocks. The silica-rich, iron-rich and melilitic lavas composes a variolitic texture lava with ovoidal segregations, submerged in a glassy or microcrystalline matrix, composed of intergrowths of needleshaped clinopyroxene – diopside, wollastonite, less commonly hedenbergite, rarely augite and labrador crystals, with brown altered glass, Fe-rich olivine – favalite is relatively less common.

Variolitic lavas are widely distributed in the Kildyam andesite succession [16]. The silicate and iron immiscibility indicated by occurrence of the varioles (globules) with different chemical compo-

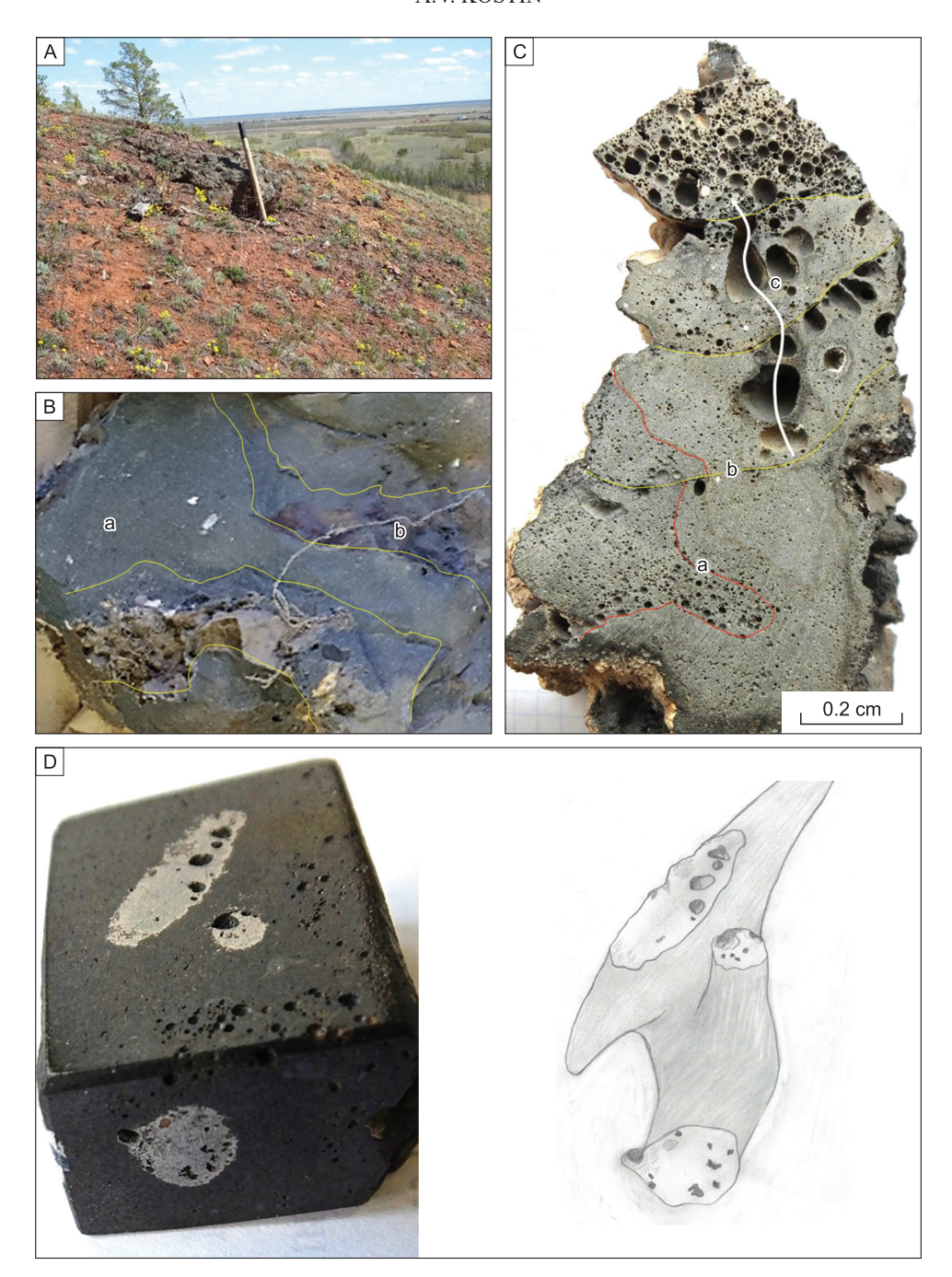


Fig. 4. Late Jurassic subvolcanic complex overlie and intrude sedimentary rocks. A – Outcrop of olivine-clinopyroxenite breccia and vivid colors of iron hydroxides in iron rich rock. B – Section through sample 1039 showing breccia of olivine-clinopyroxenite in contact with dacitic lava (location 62.284451° 129.784313° 95 m). C – Multistage carapace lavas of down-flow textural modifications, sample 1051 (location 62.285457° 129.786033° 184 m) with (a) – flow fold; (b) – lava layer shift; (c) – degassing channel. D – Polished olivine-clinopyroxenite sample with immiscible sulphide segregations of elongated morphology (a). A picture of proposal solid model for sulphide segregation (b).

sition and different matrix. First style of fractionation is a glassy dacitic lava with rare silica globules and accumulation of metallic iron (Figure 7).

Second style is an andesitic lava with numerous microlithes in glassy matrix. Globules are com-

prised of silica (rare) and magnetite (prevail) and no native iron associate with it. Titaniferous magnetite is up to 2 % by volume disseminated in the andesite matrix as mixture of ulvospinel (Fe_2TiO_4) and spinel ($MgAl_2O_4$) (Figure 8).

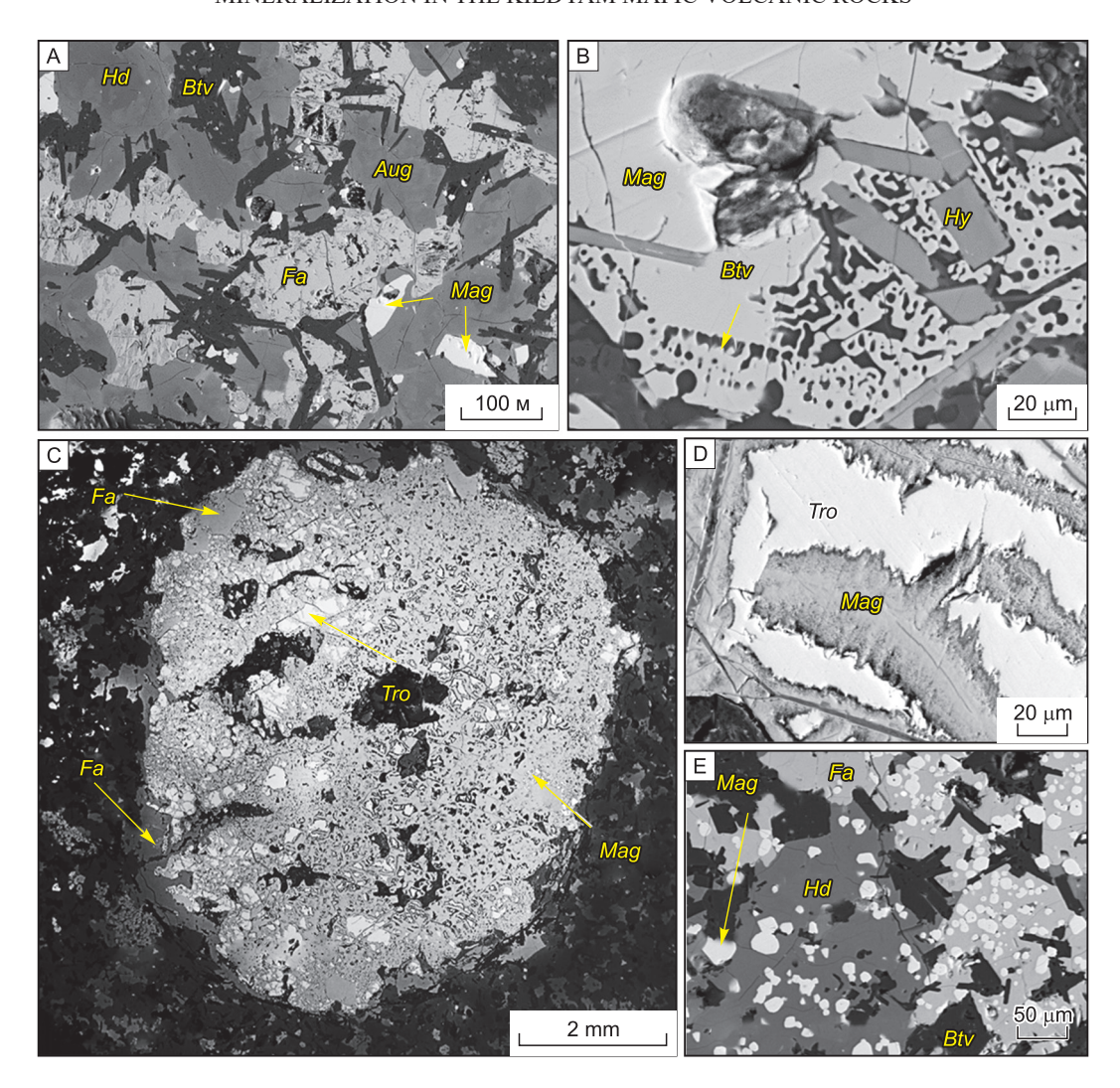


Fig. 5. A backscattered electron images showing ore minerals assemblages in the olivine-pyroxenite matrix from sample 1039 (from Kostin, 2020).

A – The relations between pyroxene, olivine, plagioclase and magnetite. Magnetite is composed of (in %): FeO_{total} – 85.38, TiO_2 – 11.16, Al_2O_3 – 2.54, MnO – 0.9. B – Intergrowth of magnetite crystal with rapid growth texture in the border and hyalophane. Hyalophane is composed of (in %): SiO_2 – 51.71, Al_2O_3 – 21.94, FeO_{total} – 1.5, CaO – 1.9, CaO –

Two minerals in andesitic lavas – fayalite and Fe-pyroxene have numerous dissolving marks and looking as outsiders. Herewith, they are both common in olivine-clinopyroxenite subvolcanic source and carapace down-flow lava textural modifications Table 4, Figure 9.

The melilitic lavas assemblage is made up of melilite mineral group – Fe-åkermanite $Ca_2(Mg,Fe^{2+})$ (Si_2O_7) (prevail) + clinopyroxene + feldspathoids + hyalophane or celsian. According to the bulk composition (in %): $SiO_2 - 36.32$, $TiO_2 - 0.62$, $Al_2O_3 - 0.62$

11.83, Fe $_2$ O $_3$ – 16.99, FeO – 4.47, MnO – 0.66, MgO – 1.95, CaO – 17.08, Na $_2$ O – 0.54, K $_2$ O – 1.16, H $_2$ O $^-$ – 1.21, H $_2$ O $^+$ – 1.8, LOI – 2.14, P $_2$ O $_5$ – 0.03, CO $_2$ – 1.62, S – 1.55 lava corresponds to melilititic and melilite-bearing volcanic rock. The magnetite-rich lava identified as titaniferous magnetite iron ore, containing magnetic fraction from 25 to 37 % of total volume and magnetite lava. All magnetite crystals trapped in the silicate matrix, composed (in %) of: SiO $_2$ – 35.5, TiO $_2$ – 0.9, Al $_2$ O $_3$ – 7.5, FeO $_{total}$ – 13.96, MgO – 3.91, CaO – 37.38, Na $_2$ O –

Table 2 Representative olivine-clinopyroxenite microprobe analyses, figure 7a (chemical X-ray maps)

Sample	SiO ₂	TiO ₂	Al ₂ O ₃	FeO _{tot}	MgO	CaO	MnO	S	Total
1039-98(01)	33.12	1.33	14.42	30.74	_	11.27	3.43	3.23	97.55
1039-98(02)	36.32	_	12.88	34.10	1.62	10.79	2.32	_	98.03
1039-98(03)	33.32	_	12.77	32.33	1.36	12.03	3.04	2.63	97.48
1039-98(04)	37.61	_	13.18	34.58	1.64	9.41	2.98	_	99.40
1039-98(05)	35.60	1.39	12.96	33.75	_	9.71	3.98	2.72	100.12
1039-98(06)	31.24	_	13.15	36.79	1.72	9.17	2.38	4.64	99.09
1039-98(07)	36.28	_	12.61	32.38	-	12.60	2.83	2.68	99.37
1039-98(08)	30.81	_	12.47	36.16	1.46	9.39	2.79	6.27	99.36

Table 3
Representative microprobe analyses of dacite glass (Figure 8B),
silica globules in dacite glass (figure 8A), andesite with accumulation of metallic iron (Figure 8C),
microlithic structure of andesitic lava (figure 9A)

						` ` `	,		
Sample	SiO ₂	TiO ₂	Al ₂ O ₃	FeO _{tot}	MgO	CaO	K ₂ O	Na ₂ O	Total
			Dac	ite glass F	ig. 8B				
1030-8(19/8)	68.06	1.37	17.80	2.72	1.98	1.00	4.13	2.53	99.59
1030-8(19/9)	68.56	_	16.83	3.00	0.91	0.74	4.61	3.96	98.61
1030-8(19/10)	65.74	0.59	17.68	3.21	1.31	2.16	3.98	3.02	97.69
1030-8(19/11)	63.31	0.95	20.13	2.42	0.77	1.39	4.36	3.87	97.2
1030-8(19/13)	67.90	1.38	18.25	2.33	2.22	1.44	4.33	3.02	100.87
1030-8(19/14)	67.27	0.71	18.69	2.99	1.31	1.57	3.81	2.90	99.25
1030-8(19/15)	64.20	0.85	19.61	3.16	1.78	_	3.96	3.85	97.41
1030-8(19/16)	64.57	1.35	18.50	2.87	1.59	1.26	3.85	3.10	97.09
		Sil	ica globul	es in dacit	e glass Fi	g. 8A			
1030-8(19/1)	99.92	_	_	_	_	_	_	-	99.92
1030-8(19/2)	99.73	_	_	_	_	_	_	_	99.73
	Ande	esite with	accumulat	tion of me	tallic iron	(1030-8)	Fig. 8C		
1030-8/01	58.12	_	15.49	3.91	1.00	15.17	2.19	2.63	98.51
1030-8/02	58.61	_	13.63	3.96	2.42	15.64	1.55	2.68	98.49
1030-8/03	57.94	_	14.10	3.53	2.11	16.84	2.10	2.12	98.75
1030-8/04	55.69	_	14.39	3.75	2.15	16.59	2.18	2.43	97.18
1030-8/05	58.15	-	15.32	4.88	2.04	15.18	2.05	2.47	100.10
1030-8/06	57.00	_	14.65	4.71	1.50	15.15	2.31	2.76	98.07
1030-8/17	56.69	1.21	15.48	4.05	1.83	14.29	2.40	3.01	98.95
1030-8/18	55.86	_	14.30	4.88	2.91	15.12	2.18	2.20	97.45
1030-8/22	57.19	1.41	13.72	5.11	3.14	14.79	1.90	2.18	99.44
	N	Iicrolithic	structure	of andesit	ic lava (10	044-7) Fig	. 9A		
1044-7(13)	61.86	_	11.71	13.11	_	5.69	3.57	1.10	97.03
1044-7(09/5)	67.10	_	10.04	13.21	_	2.06	5.71	_	98.12
1044-7(10)	61.61	_	12.50	16.55	_	5.36	3.62	_	99.64
1044-7(40/5)	69.32	_	10.29	12.49	_	1.93	5.65	_	99.67
1044-7(48/6)	57.02	_	14.23	17.61	_	4.81	3.16	_	97.67
1044-7(48/7)	56.46	_	14.55	16.35	_	5.43	2.73	_	97.36
		•			•				



Fig. 6. Namtsyr open pit exposed a full section from Late Jurassic rocks (modyfied from Kostin, 2020). A – Panorama of the quarry exposing weakly lithified sandstones, coarse-grained gritstone (1), coal (2), red tuff with flora fossils of fern and horsetail (3). B – Mined red tuff with exposed lava flows, pumice and breccia (4). C – A 1.5 m height piece of lava from the bottom of the quarry. D – Lava-breccia with quartz fragments. E – Coarse-grained gritstone fragments in lava. F – Feeder dike alters sandstone with pumice. G – Two of feeder dikes crossing sediments. H – Feeder dike altered.

0.45, $\rm K_2O-0.75$ and Figure 10. Petrographic and microprobe studies confirmed the immiscible liquids as Fe–Ti-spinel minerals group, local magnetite ore bodies. This type of magnetite comprises that of the main massive magnetite mineralization at Kildyam. In magnetite-rich lavas the FeO tot content can reach 70.8 % and ultra-rich magnetite lava contain 94.08% of FeO tot.

Dacite lava. Dacite and rhyodacite lava exposed in an upper zone, were lava flows on the slopes of the Kildyam volcano are banding and undulating. Lava unpredictably penetrate as small lava domes, composing extrusive cones. The investigated lava represent examples of different flow facies, as defined by A. Kostin and V. Trunilina in the flow emplacement

mechanisms [20]. Samples were obtained from the channel of lava that flowed northeast to feed the main flow body (sample 1058), and from several adjacent lava bodies that effused at the outboard edge of the flow (samples 1057, 1059, 1060 and 1061). All of this rock succession exposing ignimbrites of volcano vent facies, banded and wavy lavas is typical for lava flows on the slopes of the Kildyam volcano Figure 11. Ash red tuffs of rhyodacite contain fragments of uncrystallized glass, crystals and their angular fragments of acidic polysynthetically twinned plagioclase and thin angular closely soldered ash particles Figure 12.

Lava characterized by the numerous thin horizontally oriented fiamme of porphyritic black glass

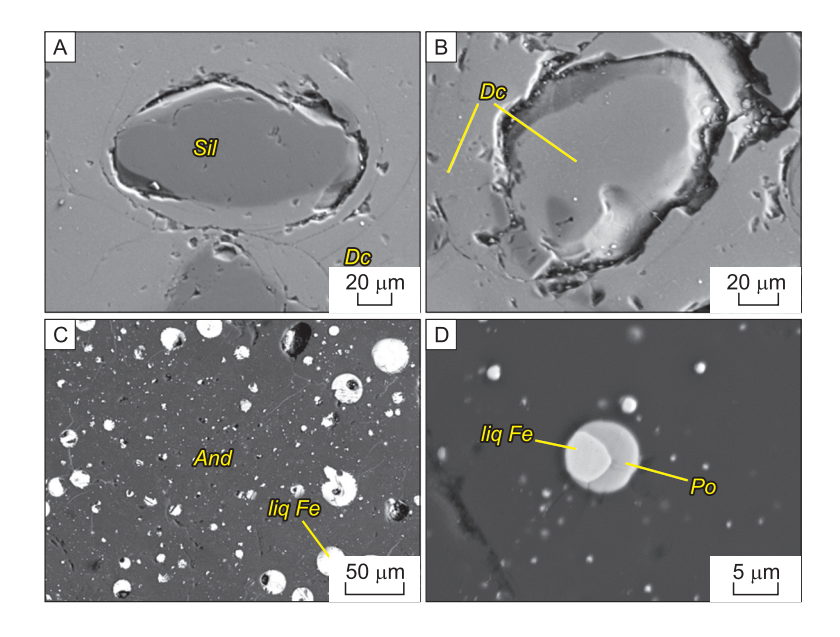
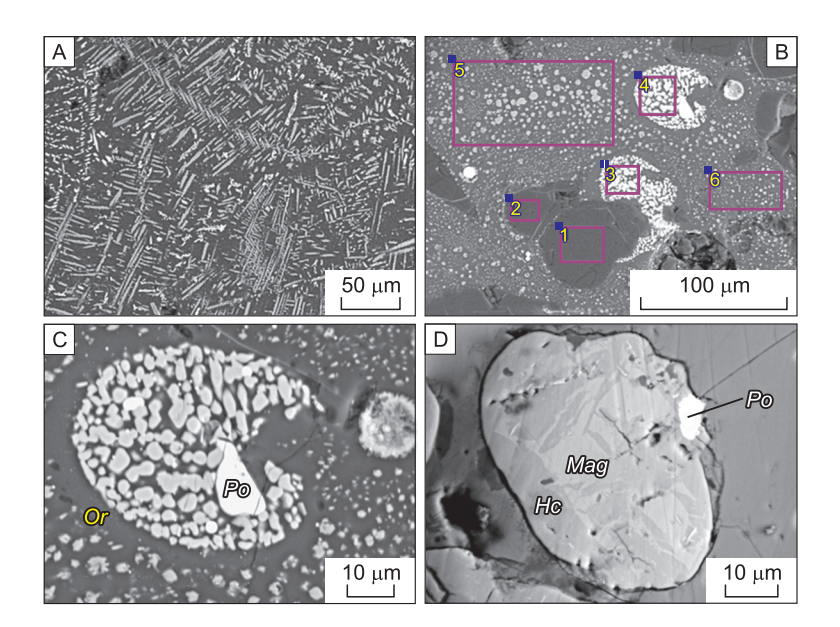


Fig. 7. Back-scattered electron images of representative dacitic and andesitic lava (first style) were a glassy dacitic lava with rare silica globules associate with accumulation of metallic iron.

A – Silica globules in dacite lava glass (1030_8/35). B – Dacite globules submerged in dacitic lava (1030_8/18). C – Andesite with accumulation of metallic iron (1030_8/1). D – Metallic iron and pyrrhotite in a globule intergrowth (1030_8/32). *liq Fe* – Native iron, *Po* – Pyrrhotite, *And* – Andesite, *Dc* – Dacite, *Sil* – Silica].



 $\begin{tabular}{l} \textbf{Fig. 8.} \begin{tabular}{l} \textbf{Back-scattered electron images and chemical X-ray maps of representative andesitic lava (second style). \\ \textbf{A}-\textbf{Microlithic structure of andesitic lava } & (1044-7/13): composition of X-ray map $SiO_2-61.86, $Al_2O_3-11.71, $FeO_{tot}-13.11, $MgO-0.76, $CaO-5.69, $K_2O-2.81, $Na_2O-1.10, $Total-97.03; microlith composition $SiO_2-52.06, $Al_2O_3-1.74, $FeO_{tot}-6.67, $MgO-1.58, $CaO-37.10, $Total-99.15.$ $B-$ Globules composition illustrate magnetite origin first, then silica, clinopyroxene phenocrysts in lava are common (1044-7/9). $Red box surrounds area of X-ray maps that are shown as insets $(1, 2-99.85-99.3 SiO_2; 3, 4-39.43-39.47 SiO_2; 46.92-46.23 $FeO_{tot}; 5.43-4.93 $Al_2O_3; 2.92-2.25 $K_2O; 1.48-1.05 $CaO; 2.55-3.37 $MnO; 5, 6-67.1-70.19 $SiO_2; 13.21-9.73 $FeO_{tot}; 9.0-9.48 $Al_2O_3; 5.71-6.49 $K_2O; 2.06-1.77 $CaO; 1.04-0.43 $MnO;). $C-Orthoclase rim around magnetite rich globule $(1044-7/8)$. $D-Two-phase globule $(1044-3/14)$ of magnetite $(FeO_{tot}-97.21; $MnO-2.7)$ and hercynite $(FeO_{tot}-51.53; $Al_2O_3-45.86; $MgO-1.87; $MnO-0.96)$. $Or-Orthoclase, $Po-Pyrrhotite, $Mag-Magnetite, $Hc-Hercynite.$ \end{tabular}$

Microprobe analyses of phenocrystals in andesite lava groundmass-glass

Sample	SiO ₂	Al ₂ O ₃	FeOtot	MnO	MgO	CaO	Total			
Fayalite										
1044-7(02)	29.95	_	60.24	4.86	2.69	_	97.73			
1044-7(04/3)	28.84	_	62.32	3.96	2.16	_	97.28			
1044-7(04/4)	31.38	_	62.07	4.40	2.07	_	99.91			
1044-7(07/2)	31.17	_	60.68	2.80	3.00	_	97.65			
1044-7(31/3)	30.54	_	63.41	2.86	2.81	_	99.61			
	•		Pyroxen	e						
1044-7(20/1)	49.50	2.17	22.24	4.61	7.53	13.25	99.29			
1044-7(20/5)	48.29	2.50	22.03	4.39	8.18	13.85	99.23			
1044-7(20/6)	48.95	2.13	22.40	4.59	7.42	14.07	99.59			
1044-7(27/1)	48.95	2.44	16.02	3.81	8.85	18.39	98.48			
1044-7(27/3)	49.14	2.43	18.22	3.10	7.31	17.98	98.18			
1044-7(27/4)	49.53	3.82	14.02	3.29	9.85	19.25	99.77			

where the glassy felsitic bulk rock is overflowed with light crystals and crystal fragments (prevail) of polysynthetically twined oligoclase-andesine, light-colored amphibole microcrystallites, pelitized sanidine and quartz. Striped and wavy lavas characterized by alternating light and dark bands with a thickness of 1–15 mm. The light bands are finely porous, with a predominance of the crystalline phase (feldspars, quartz) over the vitreous matrix, which crystallized into a microphelsite aggregate. In some cases, the dark bands represented by obsidian, in others – by bubbly to-foamy rhyodacite with larger void sizes than in the light bands and the predominance of the vitreous hyalopylite matrix over the crystalline phase.

2. Mineralization in lava globules

Iron. Several recent publications on Skaergaard intrusion and Kildyam subvolcanic [11,16] rocks indicates that iron in plagioclase increases from

0.25 to 0.45 wt% FeO $_{tot}$ with fractionation of ferrodiorites (An $_{46-32}$) in Skaergaard, and from 0.97 to 3.04 wt% FeO $_{tot}$ with fractionation of olivine-clinopyroxenite (An $_{94-54}$) in Kildyam. The evolving liquid with fractional crystallisation increased its iron content from 20.1 to 26.5 wt% FeO $_{tot}$ and its silica content from 47.4 to 49.6 wt% SiO $_2$ in Skaergaard [21] and iron content from 24.99 to 34.13 wt% FeO $_{tot}$ and its silica content from 37.44 to 45.3 wt% SiO $_2$ in Kildyam. These are important prerequisites for native iron appearense in variolitic andesites.

Major tholeiitic series in both volcanic and plutonic environments world wide are supported by occurrence of immiccible globules textures [22, 23] were native iron presents as a small droplets in plagioclase or pyroxene. Known famous provinces with Fe-rich immiccible textures are: McKinney basalt, Snake River Plain, Malad river at junction

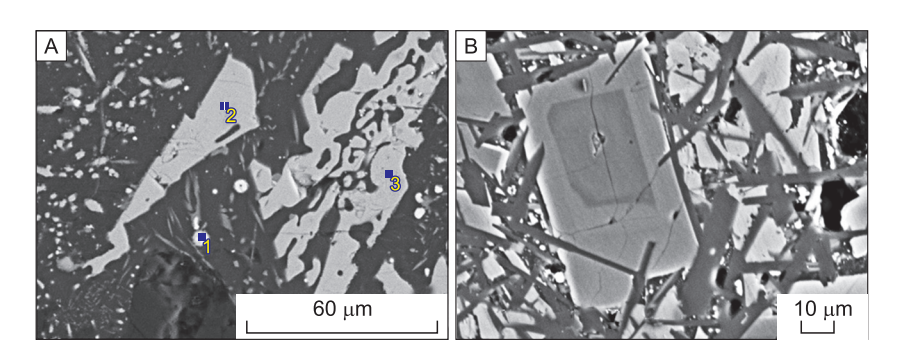


Fig. 9. Iron-rich phenocryst minerals from andesite lava evidences for olivine and clinopyroxenite minerals transition to andesite. At the same time, fayalite (A) and pyroxene (B) strongly dissolved on the migration path.

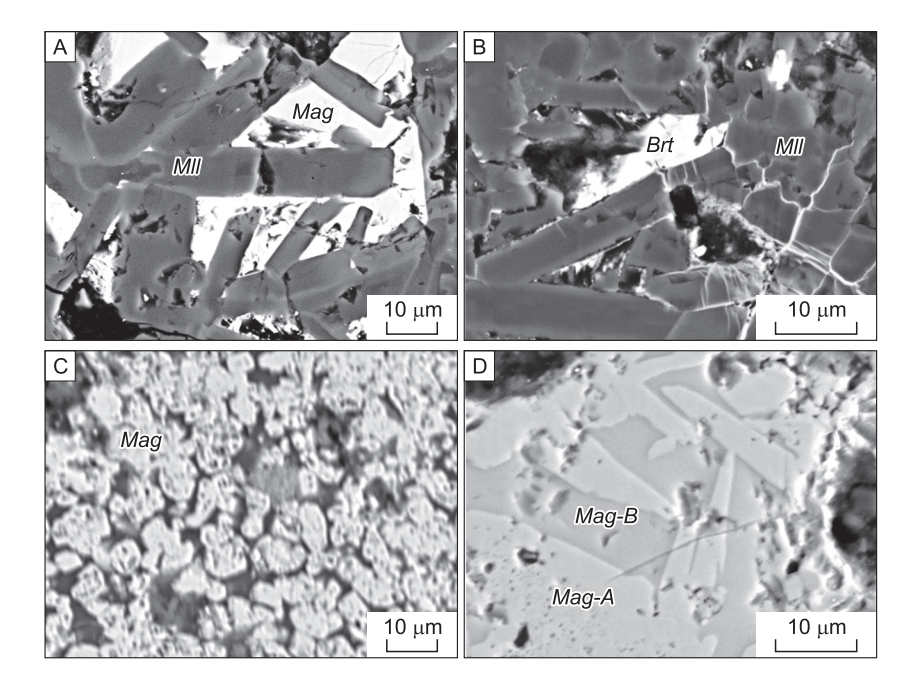


Fig. 10. Back-scattered electron images of representative melilitic and magnetite lavas [11].

A – Melilite matrix filled with magnetite. B – Depleted with magnetite melilite matrix with rare barite. C – Magnetite-A – main mineral phase; represented by fused grains of early-phase magnetite, the space between the grains is not filled. D – Late recrystallization of magnetite into Mn- and Al-Ti-rich phases Brt – Barite; Mag – Magnetite; Mag-A – Magnetite; Mag-B – Magnetite; Mll – Melilite.

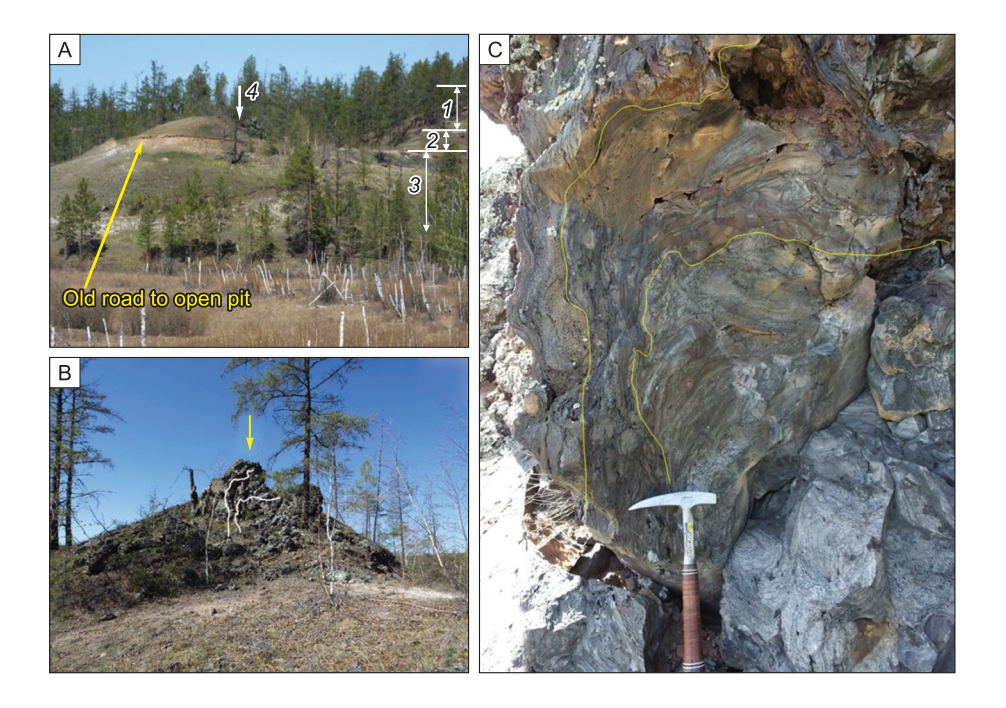


Fig. 11. Dacite extrusive cone and scoria forms the silicic eruptive sequence.

A – Volcanic cone with a diameter of 180 m (location 62.263333° 129.692529°) exposed in small open pit. Volcanic structure represented by an extrusive dome and volcanic breccias on the edges, accumulations of pumice and scoria. The top-down section presented: I) Anneal sandstone in the sole of the layer brecciated. The sandstone fragments cemented by a lava flow, indicating that the lava has penetrated under the flow. 2) Lavabreccias are represented by fragments of anneal sandstone displaced and cemented with lava flow. 3) Volcanic flows composed of glass, banded lavas, lava breccias, pumice stones, and carapase. 4) An extrusive volcanic cone with the texture of the lava flow streaming rises up the vent and then falls on its side. B – Dacite extrusion - protruding viscous lava forms a column about 4 m high above the cone. C – Bending of the dacite lava flow from a feeder channel.

MINERALIZATION IN THE KILDYAM MAFIC VOLCANIC ROCKS

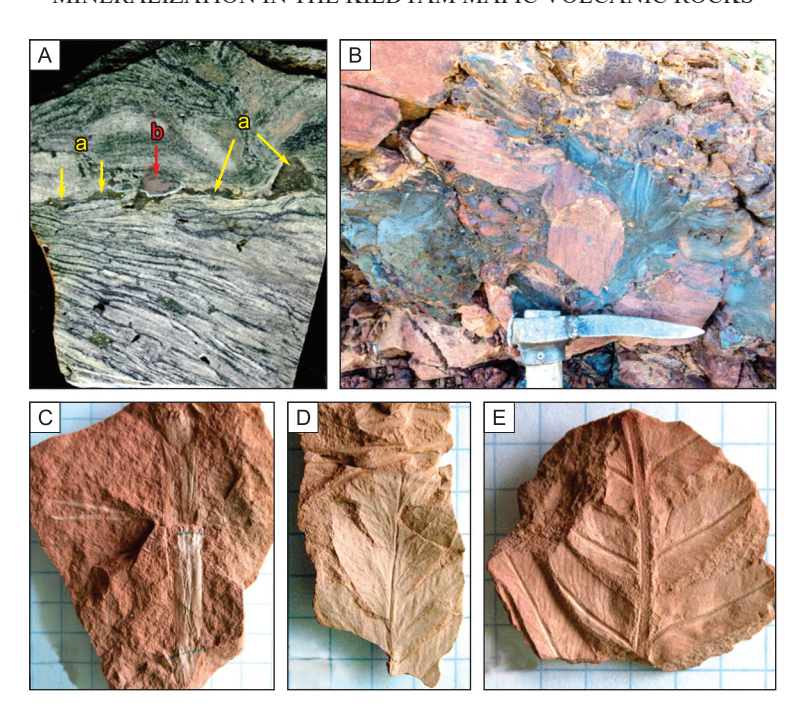


Fig. 12. Riodacite lava and red tuff exposing in the upper volcanic zone.

A – Riodacite ignimbrites (sample 1044/3, location 62.263997° 129.716967°) introduced with light fragments of cristaloclastic porous lava and black elongated scraps and lenses of glass. On the ignimbrite border scraps of a fayalite – bytownite - hedenbergite (a) and fayalite–hercynite–hematite (b) from subvolcanic complex. B – Reddish tuff brecciated and cemented with ignimbrites.

C–E – The fossils of Late Jurassic flora in brick-red crystalloclastic tuffs from Kildyam volcanic succession [15]. C – Equisetites cf. acmophyllus Kiritch. B and F – Cladophlebis aldanensis Vachr.

with Snake River, Idaho [24]; Olivine basalt from Blowsa quarry, Tansa, Bombay, Deccan traps [25], Basalt from Jokulsa a Fjöllum, Iceland [26], Andesite from the 1845 lava of Hekla volcano, Iceland [27]. Since 2018 Fe-rich and Si-rich immiccible textures were dickovered in the Kildyam volcanic complex, Yakutia: (a) phenocrysts of plagioclase and wollastonite in andesite microlite matrix were labrador saturated with small droplets of native iron; (b) labrador filled with micro-spherules of native iron; (c) immiscible texture in glass and hedenbergite microlites, plagioclase is free of liquid iron micro-spherules; (d) immiscible texture in needle secretions of hedenbergite and phenocrysts of in plagioclase (labrador); (e) a drop of native iron in pyrrhotite; (f) spherical separation of pyrrhotite with fused drops of native iron inside.

Variolitic lavas of Kildyam mineral assemblage with native iron, include different amount of magnetite, troilite, pyrrhotite and pyrite, and is considered common in the tholeite trap formation of the Siberian platform [28]. Native iron occurs as a large segregations and drops in the rock-forming andesites and in the phenocrysts of plagioclase and pyroxene Figure 13. Impurities of Co – 0.04–2.89 %; Ni –

0.01-1.09 %; Pt – to 1.45 %; Ir – to 2.97 % are installed in native iron.

3. Mineralization in lava vesicles

Mineralized vesicles in lava are usualy grouped in chains are connected with cracks. Most of them are hollow and only some of them are filled with cristobalite, metallic sublimates, sulphides and iron-oxides. The metallic sublimates in the vesicle walls of mafic volcanic lava are morphologically and compositionally similar among the volcanoes. Based on microprobe analyses, the major of ore bearing vesicles content in Kildyam Volcanic Complex are Cu–Zn, Al–Fe–Cu and Fe–Ni–Cu–Sn alloys, Ag, Zn, Pb, Fe and Cu, Ag sulfides. Among diagnosed sulphides are Ag-tetrahedrite, argentite, galena, sphalerite, chalcopyrite, pyrite, troilite. Most common mineral in volcanic vesicles is cristobalite.

Cristobalite. Cristobalite is a low-pressure high-temperature polymorph of SiO₂ in many styles of volcanic rocks. This is typical of rapidly cooled effusive rocks, usually tends to the upper parts of basaltic, andesitic, and dacitic lava structures, and may occupy more than 10% of the rock volume, but is not a primary magmatic phase. Cristobalite is commonly found in the dome lava as a post volcanic phase. The

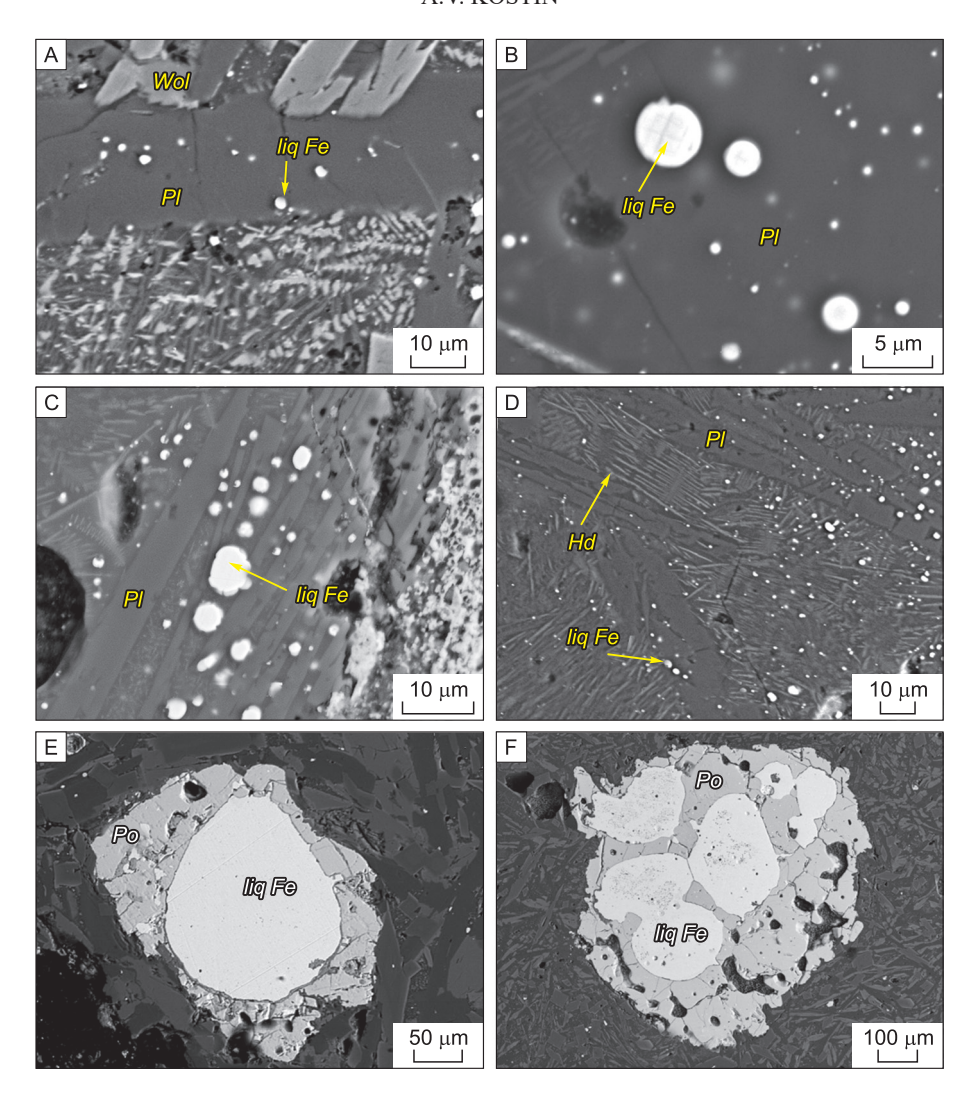


Fig. 13. Back-scattered electron images of immiscible textures in Kildyam volcanic rocks. A – Phenocrysts of plagioclase (labrador) ([Na $_{0.388}$ Ca $_{0.662}$] $_{1.1}$ (Al $_{1.54}$ Si $_{2.409}$) $_{3.9}$ O₈-SiO $_2$ – 53.63, Al $_2$ O $_3$ – 29.08, CaO – 13.76, Na $_2$ O – 4.46, Total-100.92) and wollastonite ({Ca $_{0.991}$ } $_{1.0}$ [Fe $^{2+}$ $_{0.09}$ Mg $_{0.666}$ Al^{VI} $_{0.201}$] $_{1.0}$ (Si $_{2.053}$) $_{2.1}$ O₆-SiO $_2$ – 54.93, Al $_2$ O $_3$ – 4.56, FeO $_{tot}$ – 2.89, MgO – 11.95, CaO – 24.74, Total – 99.07) in andesite microlite matrix. Labrador saturated with small droplets of native iron. B – Labrador filled with micro-spherules of native iron. C – Immiscible texture developed in glass and hedenbergite microlites. Plagioclase is free of liquid iron micro-spherules. D – Immiscible texture developed in needle secretions of hedenbergite (SiO $_2$ – 54.61, Al $_2$ O $_3$ – 2.44, FeO $_{tot}$ – 18.44, MgO – 5.11, CaO – 18.20, Total – 98.80 {Ca $_{0.780}$ Fe $^{2+}$ 0.036} $_{0.88}$ [Fe $^{2+}$ 0.580Mg $_{0.305}$ Al^{VI}0.115] $_{1.0}$ (Si $_{2.184}$) $_{2.2}$ O₆) and phenocrysts of in plagioclase (labrador). E – A drop of native iron in pyrrhotite. F – Spherical separation of pyrrhotite with fused drops of native iron inside Hd – Hedenbergite; Iiq Fe – Native iron; Po – Pyrrhotite; Wol – wollastonite.

examples of San Cristobal (Mexico) by Horwell C.J. et al., Maina in Rhineland (Germany) by Reich M. et al., Yellowstone Park (USA) by Schipper C.I. et al. and in many other, make sure that presence of cristobalite indicates gas phase activity after the eruption [29–31].

Total amount of cristobalite in the Kildyam extrusive domes can reach 5 %. Kildyam post volcanic phase is composed of cristobalite (prevail), quartz and mullite. Due to high temperature of postmagmatic degassing cristobalite usualy do not associate

with sulphides. Accumulations of cristobalite found in the voids of olivine-clinopyroxenite, andesite and dacite lavas (Figure 14). Cristobalite is always detected in large stretched vesicles of lava flows close to volcanic dome structures. Elongated or spherical vesicle shape of bubbles indicate (A) mooving lava flow down the slope; (B) lava fills relief and stop mooving.

Alloys. To better understand how copper alloys rise through the lava using vapour bubbles, we studied Cu mineralisation in different vesicles of mafic

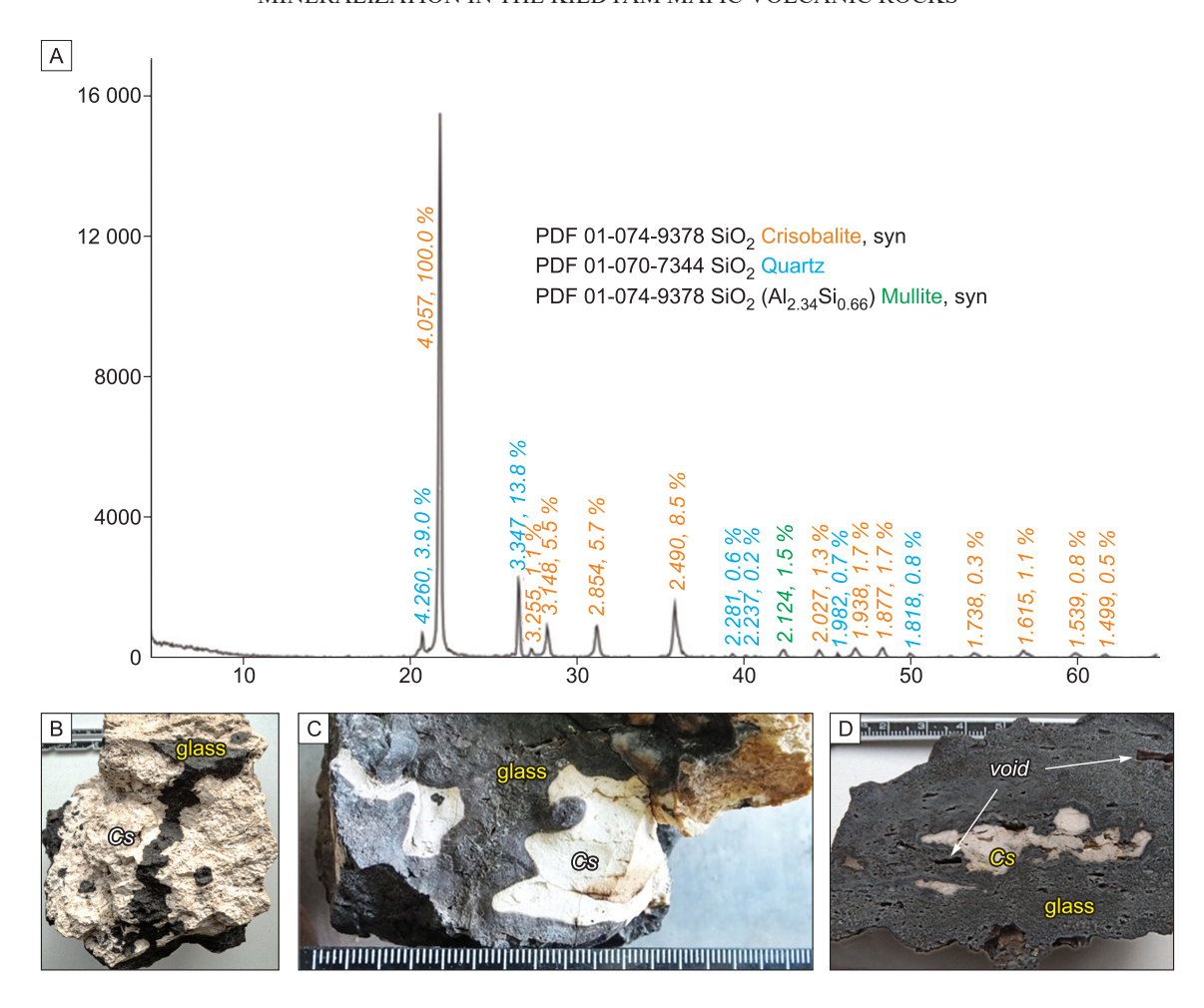


Fig. 14. Different sample styles for cristobalite in Kildyam lavas (determined by x-ray phase analysis using D2 PHASER Bruker diffractometer, CuKα radiation, 30 kV, 10 ma and database PDF-2 with Diffrac.Evaluation Package). A – Diffractogram showing a mineral mixture of cristobalite, quartz and mullite. B – Cristobalite apparently filling all available void space (sample 1051/2). C – Different shape of voids filled with cristobalite (sample 1051/3). D – At a distance from dacitic dome some void space in lava available (sample 1051/4).

lava and scoria from Kildyam succession. As reported here, Cu-alloys have compositional variations for diverse lava systems. Copper alloys are most common in highly vesicular andesite and magnetite lava. The Kildyam eruptive products contained an abundance of Fe-Ti oxides in groundmass and Cu-alloys within the vesicles. Cu-alloys come in many shapes depending on alloy amount and vecicle volume, many of them are gold in color and not easily confused with any silic minerals Figure 15.

Metal alloy grains are attached to a vesicle walls with anorthoclase (Figure 15A, B), magnetite (Figure 15C) and silica poor glass (Figure 15D). Many of described alloys in vesicles of mafic volcanic rocks indicate wide transport and depositing of Cu–Au, Cu–Fe, Co–Fe–Ni, Cu–Sn–Co, Cu–Sn–Co–Ag (Etna), Ag–Sn–Fe, Cu–Sn–Co (Vesuvius), Fe–Cr–

Ni, Au, Cu–Pb–Zn, Cu–Sn–Co (Stromboli), Bi–Cu, Ni, Au–Fe, Bi, Cu–Sn–Co (Kilauea), Tolbachic [5, 6, 32, 33]. From 2018 to 2020 field studies at the eruptive products of Jurasic Kildyam succession we found alloys with distinct compositional variations for each lava style. Andesitic lava with vesicle in anorthoclase surrounding and Cu–Zn alloy attached to a vesicle wall (sample 1030_1/011). Crystalized magnetite lava with less glass and detached Fe–Al–Cu alloy from the wall (sample 1064_1/08). Ironrich glass lava with Ni-Fe-Cu-Sn alloy in detached from the wall vesicle too (sample 1064_2/10).

Sulfides. Porous balls, filled with Fe, Fe-K and Cu-Fe sulfides found from Kildyam, are similar to those described in many volcanic world locations [33–35]. Balls contain subspherical agglomerations interpreted as amygdules, partly or completely filled with

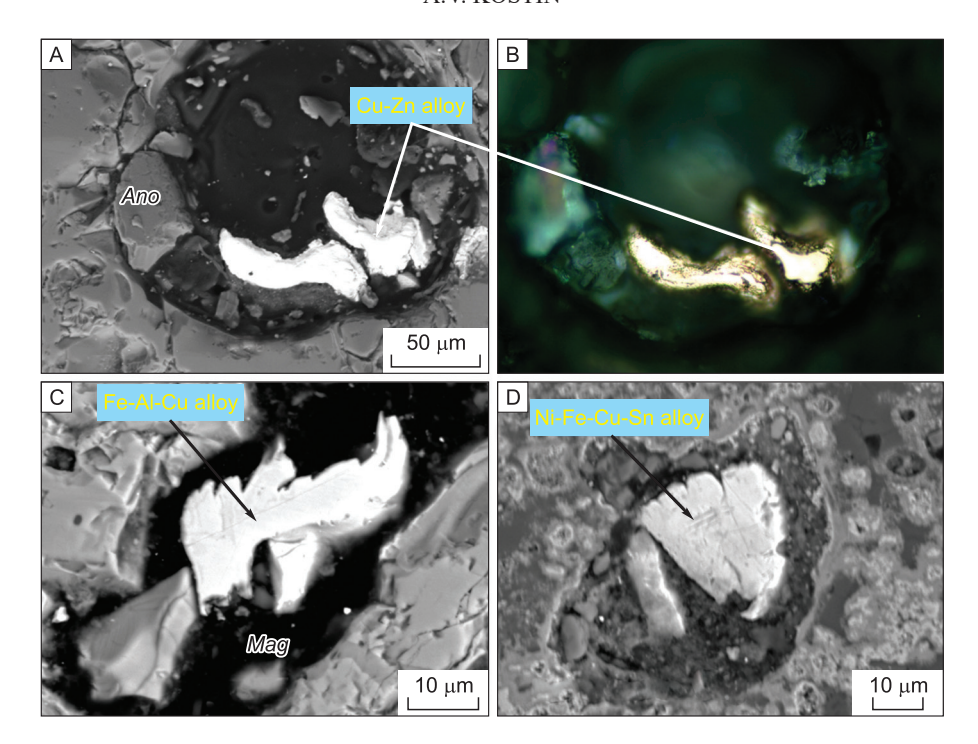


Fig. 15. Detail back-scattered electron images (A, C and D) and microphotograph in reflected light (B) of copper alloys in lava vesicles.

A and B – Vesicle in andesitic lava with anorthoclase surrounding. Cu–Zn alloy is in gold color (sample $1030_1/011$). C – Vesicle surrounded with magnetite (FeO_{tot} – 99.05, MnO – 0.65) + glass (FeO_{tot} – 56.8, MgO – 9.37, CaO – 4.17, MnO – 29.39, Total – 99.73) are composed of Fe-Al-Cu alloy (sample $1064_1/08$). D – Vesicle in iron-rich glass (SiO₂ – 39.23, Al₂O₃ – 8.06, FeO_{tot} – 46.67, TiO₂ – 0.97, MgO – 0.54, Na₂O – 0.9, K₂O – 0.74, Total – 97.11) with Ni–Fe–Cu–Sn alloy (sample $1064_2/10$). Ano – anorthoclase, Gl1 – iron rich glass, Mag – Magnetite, Mll – melilite.

Microprobe analyses of copper mineral assemblage in magnetite lava vesicles from Kildyam Volcanic Complex

Al	Fe	Ni	Cu	Zn	As	Sn	Total			
Cu ₂ Zn (tongxinite)										
_	_	_	66.05	33.62	_	_	99.67			
-	_	_	66.13	34.24	_	_	100.37			
_	_	_	65.65	33.66	_	_	99.31			
_	_	_	66.69	33.09	_	_	99.78			
			Fe–Al–Cı	ı (alloy-1)						
12.95	4.17	_	83.26	_	_	_	100.38			
8.27	3.94	_	87.73	-	_	-	99.94			
12.24	4.37	_	83.19	_	_	_	99.8			
8.61	4.1	_	84.23	_	_	_	96.94			
7.15	4.22	_	86.64	_	_	_	98.01			
10.1	4.32	_	85.93	_	_	_	100.35			
	Ni–Fe–Cu–Sn (alloy-2)									
_	16.03	14	34.69	_	_	30.62	95.34			
_	23.39	11.18	36.96	_	_	24.03	95.56			

Table 5

MINERALIZATION IN THE KILDYAM MAFIC VOLCANIC ROCKS

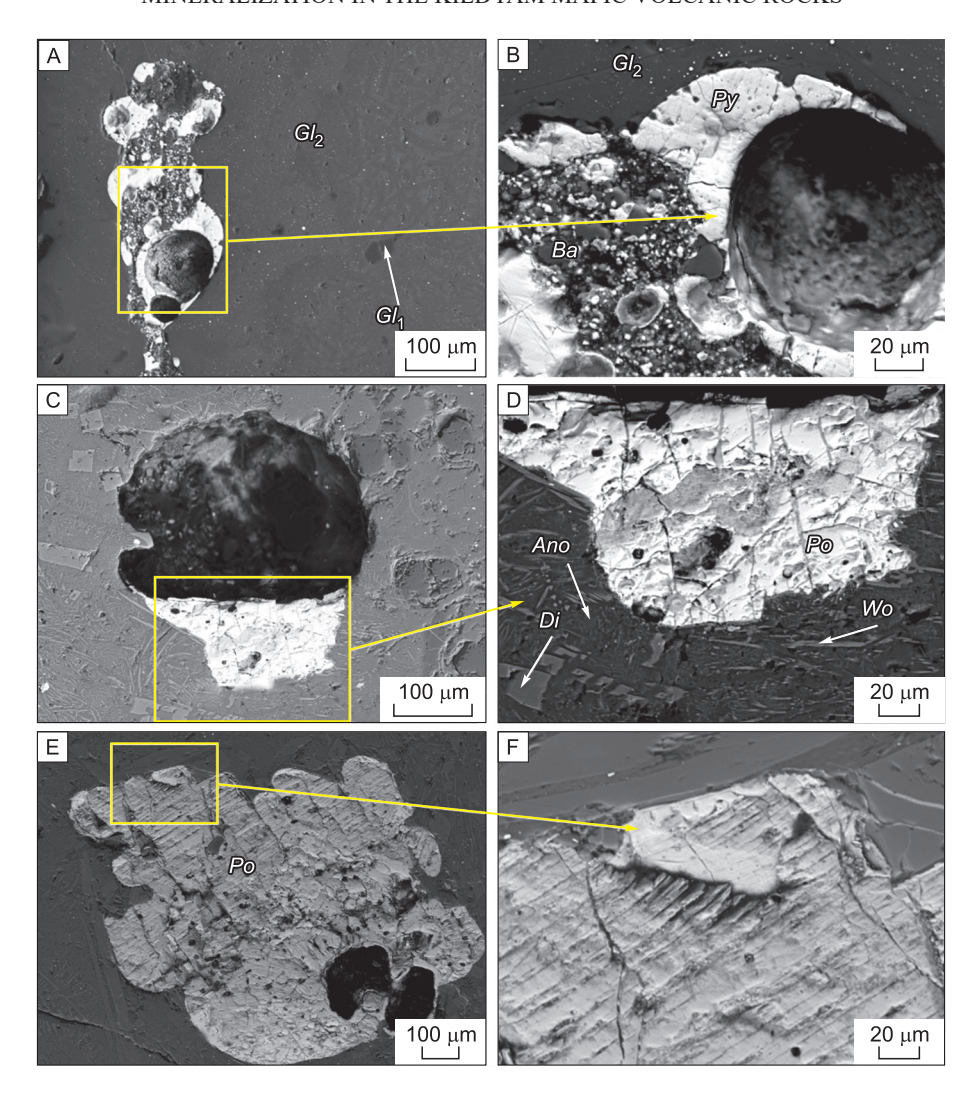


Fig. 16. Back-scattered electron images showing general forms and details of vesicles with iron sulphides saturation in andesite lava [11].

A, B – Rising assemblage of porous balls of pyrite and bartonite in andesitic lava, due to the speed of bubble formation, occur foaming and rapid solidification (general view and details, samples 1030-8\027-028). C, D – Sulfide-silicate liquid immiscibility leads to accumulation of heavy sulfide minerals in the lower part of the bubble; in many cases, these globules partially fill subspherical intercumulus spaces within vesicle with sulfides (general view and details, samples 1030-1/033-034). E, F – Bubbles completely filled with pyrrhotite and troilite represent the heaviest ore style in the lower parts of the lava flows (general view and details, samples 1030-1/026-027). *Ano* – anorthoclase, Ba – bartonite, Di – diopside, Gl1 – silica variole, Gl2 – glass with plagio-clase phenocrysts, Po – pyrrhotite, Py – pyrite, Tro – troilite, Wo – wollastonite.

sulfide minerals (pyrrhotite, troilite, pyrite, chalcopyrite, bartonite); in places amygdules form elongated clusters (general view and details) (Figure 16A, B). Often gas bubbles occupy very large volumes, there are not enough sulfides, and the voids only partially occupied. Rising assemblage of porous sulfide balls in andesitic lava (Figure 16C, D). The rarest bubbles completely filled with sulfides; consisting mainly of pyrrhotite and less often troilite (Figure 16E, F).

Sulfide melts are presented in three forms; (1) as sulfide phases in olivine-clinopyroxenite (about

89 mol% of Fo) melt, (2) sulfide inclusions hosted by andesite lava, and (3) inclusions in interstitial to the groundmass (pyroxene, plagioclase, and magnetite) minerals. Kildyam sulfide liquids enriched in Au-0.21-3.15, Ag-0.15-1.68, Pt-0.52-2.88 (outcrop 1039); Au-0.1-2.71, Ag-0.11-1.47, Pt-0.04-3.36, Pt-0.04-2.89, Pt-0.01-1.09 (outcrop 1030).

In 2015–2020, sampling program successfully discovered unknown sulfide mineralization [11, 14, 16]. By now, chalcopyrite is a minor ore mineral, but the

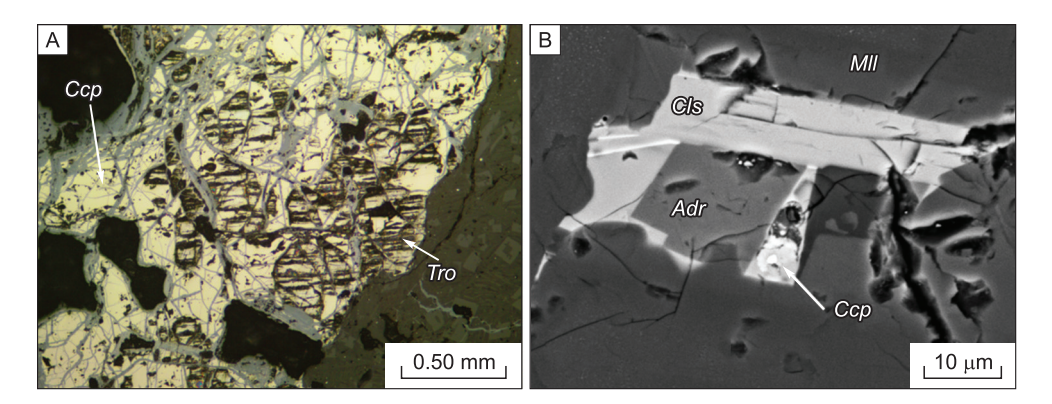


Fig. 17. Diverse copper mineral associations in chalcopyrite-troilite and mineralised melilitic rocks. A – Close-up photomicrograph of chalcopyrite-troilite intergrowths in the bottom of a vesicle in olivine-clinopyroxenite (sample 1039). B – Melilitite with less celsian and androdite chalcopyrite spherule (sample 1064-3). *And* – androdite, *Ccp* – chalcopyrite, *Cls* – Celsian, *Mll* – melilite, *Tro* – troilite.

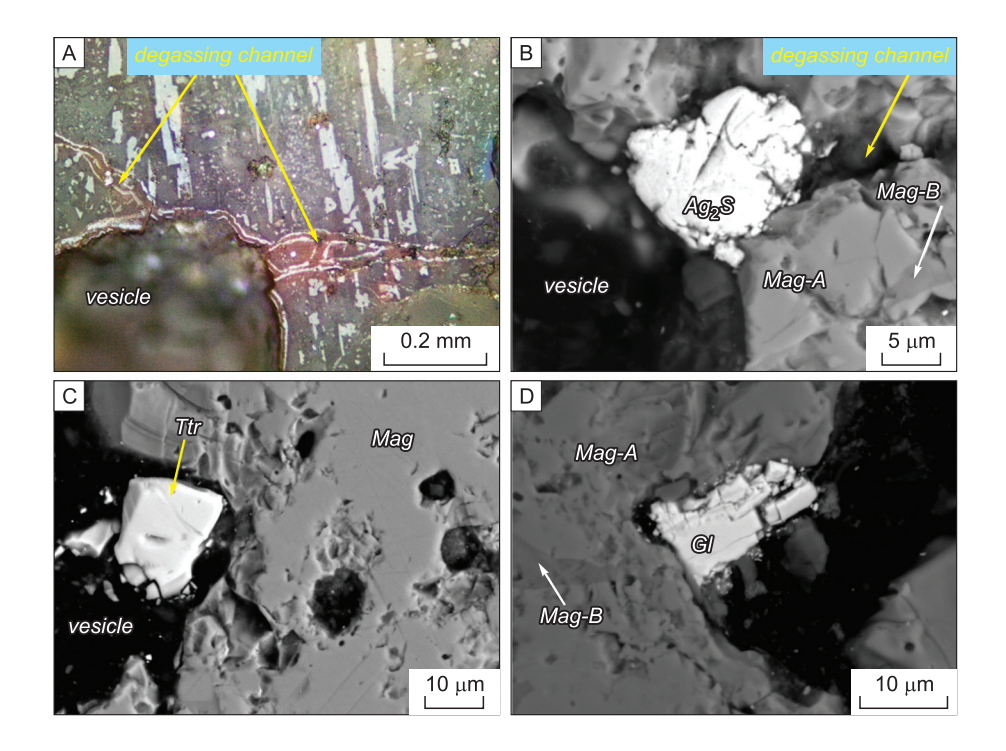


Fig. 18. Typical ovoid morphology for the vesicle structure in the andesitic lava and associated degassing channels with the sulfide sublimates.

A – Optical reflected light microphotograph of mineralized vesicles in andesitic lava. Vesicles and degassing chanels are grouped in chains and connected with cracks, filled with sulfides sublimates, iron-oxides and cristobalite. B–D – Back-scattered electron images showing silver and led minerals in the magnetite lava vesicles. B – Crystal of Ag-tetrahedrite (sample 1064-1-16); C – Grain of Cu-Fe-argentite (sample 1064-1-06); D – Galena grain. Ag2S – Argentite, Gl – Galena, Mag – Magnetite, Mag-A – Magnetite; Mag-B – Magnetite; Ttr – Tetrahedrite.

situation may change due to the discovery of new ore-bearing structures. Occurrence of diverse copper mineral associations in the Kildyam volcanic succession documented in (A) complex shaped and sized globules hosted of chalcopyrite-troilite inter-

growths in olivine-clinopyroxenite, and (B) globular disseminated chalcopyrite in mineralised melilitic rocks; chalcopyrite is armored (completely encased in a silicate phase) in plagioclase and pyroxene Figure 17.

Table 6

Kildyam sulfides in different volcanic occurrence

Sample	S	K	Fe	Со	Ni	Cu	As	Total			
1	2	3	4	5	6	7	8	9			
			Pyrrhotit	te (Fe ²⁺ _{0.95}	S)						
	From ore globules in pyroxenite matrix										
1039-1(2/2)	38.39	_	60.03	1.13	0.09	0.36	_	100.00			
1039-1(2/7)	38.16	_	60.93	0.88	0.13	0.34	_	100.14			
1039-1(4/5)	39.53	_	58.97	0.44	0.43	_	_	99.37			
1039-1(4/8)	38.61	_	59.80	0.13	_	0.11	_	98.65			
1039-1(4/9)	38.93	_	59.29	0.59	0.23	_	_	99.04			
1039-1(6/1)	38.49	_	59.30	1.58	0.31	0.53	_	100.00			
1039-1(6/5)	38.28	_	59.30	1.58	0.31	0.53	_	100.00			
1039-1(6/6)	37.79	_	58.88	0.75	0.62	0.31	_	98.36			
1039-1(6/7)	38.19	_	59.74	0.36	0.09	0.21	_	98.59			
1039 (4/1)	38.69	-	61.22	0.11	0.11	0.38	_	100.52			
1039 (6/1)	38.59	_	59.48	0.73	0.09	0.69	_	99.58			
		From surr	ounding o	f iron liqui	ds in andes	site					
1030-1(2/1)	38.60	_	61.31	0.49	0.14	0.21	_	100.76			
1030-1(2/4)	37.15	_	61.41	0.69	_	0.11	_	99.36			
1030-1(14/2)	37.16	_	61.60	0.65	0.21	_	_	99.62			
1030-1(16/1)	38.06	_	60.41	0.46	0.30	0.69	_	99.93			
1030-10(31/2)	35.59	_	61.39	0.65	1.23	0.66	_	99.52			
1030-10(31/5)	35.87	_	60.94	0.42	_	0.23	_	97.45			
			Troili	te (Fe ²⁺ S)							
		Fron	n the bubbl	e edges in	andesite						
1030-1(27/1)	36.22	_	64.02	0.14	_	0.22	_	100.59			
1030-1(3/2)	36.09	_	63.90	0.12	0.32	0.07	_	100.50			
1030-1(7/1)	37.33	_	62.43	0.39	0.11	_	_	100.26			
1030-1(7/2)	34.03	_	63.01	1.44	0.45	0.24	_	99.17			
1030-1(8/1)	36.71	-	62.87	0.22	0.39	0.29	_	100.48			
1030-1(8/2)	36.28	-	63.08	0.22	0.44	_	_	100.02			
1030-1(8/4)	36.31	_	64.16	0.18	0.09	0.14	_	100.89			
1030-1(8/5)	36.58	_	63.53	0.46	0.10	_	_	100.68			
1030-1(9/5)	37.08	_	62.39	0.41	0.31	0.17	_	100.47			
1030-1(10/1)	37.66	_	62.59	0.16	0.39	0.12	_	100.92			
1030-1(15/2)	35.25	_	63.55	0.39	0.23	0.20	_	99.63			
		From	drops of ire	on liquids i	n andesite						
1030-10(18/2)	36.29	_	63.16	0.28	0.39	0.48	_	100.60			
1030-10(18/3)	36.11	_	63.48	_	_	0.02	_	99.61			
1030-10(18/4)	35.45	_	62.99	0.29	_	_	_	98.73			
1030-10(18/5)	35.68	_	62.82	_	0.59	0.70	_	99.80			
1030-10(19/4)	35.67	_	63.27	0.71	_	0.23	_	99.86			
1030-10(19/7)	34.96	_	62.60	1.10	0.09	0.17	_	98.93			
1030-10(25/1)	35.57	_	62.89	0.47	0.36	0.16	_	99.44			
1030-10(29/2)	35.69	_	62.99	0.86	_	0.16	_	99.70			

1	2	3	4	5	6	7	8	9			
1030-10(33/2)	33.68	_	64.67	0.28	0.38	_	_	99.01			
	Pyrite (Fe ²⁺ S ₂)										
From the bubble edges in andesite											
1030-1(27/1)	54,42	_	44,49	_	_	_	_	98,91			
1030-1(27/2)	56,11	_	42,95	_	_	_	_	99,06			
1030-1(27/3)	52,49	-	44,60	_	_	_	_	97,09			
	Bartonite $(K_3Fe^{2+}_{10}S_{14})$										
			From bubb								
1044-7(35/1)	39.35	9.76	49.77	_	_	_	_	98.88			
1044-7(35/2)	39.39	9.02	50.31	_	_	_	_	98.72			
1044-7(35/3)	40.59	9.82	47.12	_	_	_	_	97.52			
1044-7(35/4)	40.26	8.80	49.51	_	_	_	_	98.57			
1044-7(35/5)	40.05	9.36	48.56	_	_	_	_	97.97			
1044-7(35/6)	39.89	8.82	49.47	_	_	_	_	98.18			
			Chalcopyr	rite (CuFe ²⁻	+S ₂)						
	From liquids in melilitite										
1064-3(16/1)	34.15	_	33.05	_	1.62	26.91	4.78	100.51			
1064-3(16/2)	34.74	_	39.93	_	1.06	20.32	1.63	97.68			
1064-3(16/3)	34.88	_	31.43	_	1.64	26.94	3.92	98.81			

Table 7
Microprobe analysis of Ag-minerals in vesicles from magnetite lava, in % (from [11])

Sample	Cu	Ag	Fe	Zn	Sb	As	S	Total			
Ag-tetrahedrite											
1064-16	31.71	6.10	5.72	4.07	25.96	2.39	23.41	99.36			
1064-16	31.71	6.19	5.08	5.82	24.72	1.74	24.45	99.71			
1064-16	32.31	6.06	5.64	5.33	24.27	2.14	23.84	99.59			
1064-16	31.33	6.35	6.44	4.48	22.75	2.2	24.71	98.26			
1064-16	31.58	5.73	5.03	4.07	25.34	1.44	24.11	97.30			
1064-16	32.79	5.71	5.28	5.97	26.17	1.46	22.01	99.39			
1064-16	32.37	5.72	5.41	3.56	25.78	1.43	24.77	99.04			
			Cı	ı-Fe-argent	ite						
1064-06	3.95	78.22	2.27	_	_	_	15.18	99.63			
1064-06	3.49	78.77	2.50	_	_	_	14.62	99.38			
1064-06	3.62	79.26	1.23	_	_	_	13.16	97.27			
1064-06	1.93	79.00	2.92	_	_	_	14.21	98.07			
1064-06	2.51	79.32	2.49	_	_	_	14.64	98.97			

Our results support igneous vapor transport of antimony-silver-copper-led-iron-zinc-sulfur into silver minerals system, and imply preconcentration in mafic volcanic system during lava solidification. Among diagnosed sulphides are Ag-tetrahedrite, argentite, galena, chalcopyrite, pyrite, troilite; two of silver minerals – Ag-tetrahedrite and Cu-Fe-argentite diagnosed in the andesitic lava vesicles (Fi-

gure 18, Table 6 and Table 7) [11]. A degassing model envisions initial Ag enrichment in crystallizing interstitial liquid and further enrichment in a separating vapor phase Figure 18A.

Conclusions

Low S content in the Kildyam magma come initially from fayalite, clinopyroxene, plagioclase and

magnetite parent magma. All Kildyam volcanic processes somehow occur in connection with the iron enrichment, (1) during the early stage of fine-grained subvolcanic olivine-clinopyroxenite end pyrrhotite; globular igneous sulfides is a first proposed style of economic deposit formation, (2) the second proposed style of economic mineralization in Kildyam is to be a magnetite-bearing lava; iron enrichment of the melilitic melt phase, followed by iron depletion and silica enrichment. Kildyam magnetite crystallization mark the end of absolute iron enrichment in magma, the same way as in the Skaergaard intrusive [36]. Accumulation of large sulfide volumes, fayalite and augite near the surface, indicate possibile existence of substantially heavier rocks located deeper. This is confirmed with a presence of an unusual complicated mineral phase of spinelide, discovered in andesite-variolitic lavas; it is a mix of ulvespinel $(Fe_2TiO_4) \pm spinel (MgAl_2O_4)$, enriched with Nb. Back-scattered electron image show fragments of ulvospinele skeletal crystal in glass matrix, which most likely came from olivine-clinopyroxenite.

The vesicle-hosted alloys and sulfides provide significant new data on metal transport and precipitation from high-temperature magmatic vapors. During syneruptive vapor phase exsolution, (3) volatile metals (Cu-Zn, Fe-Al-Cu, Ni-Fe-Cu-Sn) and Ag-Cu-sulfides contribute to the formation of economic concentrations. Our research confirmed that tholeiitic trend of iron-rich olivine-pyroxenites evolves towards two immiscible liquids - magnetite lava and melilitite matrix. Further evolution lead to the separation of native iron and the transition of lavas to the silicarich calc-alkaline trend. Petrographic and microprobe studies confirmed the liquid immiscibility in silicate melts during crystallization. Immiscible liquids are preserved as globules of one glass in another in andesites and as melted inclusions of native iron in matrix, clinopyroxene and plagioclase phenocrysts.

Author Contributions

The author express his gratitude to Olga Fomenko, Professional Geoscientist Ontario, Golder Associates Ltd. for her constructive comments and excellent suggestions that helped to improve the manuscript. I am grateful for the support of the idea of studying the Kildyam Volcanic Complex and numerous discussions on all aspects of volcanism to the Institute colleagues – Vera A. Trunilina, Oleg B.

Oleinikov, Vitaliy S. Grinenko, and Maria S. Jelonkina. Tatyana I.Vasileva is thanked for excellent x-ray analyses of volcanic rocks. Microprobe analyses were provided with the great help of Maria S. Jelonkina. Sample preparation for microscope and microprobe studies were well done by Vladimir Kurchatov.

Funding

This research was funded by Diamond and Precious Metal Geology Institute, Siberian Branch of the Russian Academy of Sciences, project number 0381-2019-004.

References

- 1. *Hattori K.H., Keith J.D.* Contribution of mafic melt to porphyry copper mineralization: evidence from Mount Pinatubo, Philippines, and Bingham Canyon, Utah, USA // Miner. Depos. Springer, 2001. Vol. 36, No. 8. P. 799–806.
- 2. *Meeker K.A. et al.* Emission of elemental gold particles from Mount Erebus, Ross Island, Antarctica // Geophys. Res. Lett. Wiley Online Library, 1991. Vol. 18, No. 8. P. 1405–1408.
- 3. *Hinkley T.K. et al.* Metal emissions from Kilauea, and a suggested revision of the estimated worldwide metal output by quiescent degassing of volcanoes // Earth Planet. Sci. Lett. Elsevier, 1999. Vol. 170, No. 3. P. 315–325.
- 4. *Allard P. et al.* Acid gas and metal emission rates during long-lived basalt degassing at Stromboli volcano // Geophys. Res. Lett. Wiley Online Library, 2000. Vol. 27, No. 8. P. 1207–1210.
- 5. *Hunter E.A.O. et al.* Vapor Transport and Deposition of Cu-Sn-Co-Ag Alloys in Vesicles in Mafic Volcanic Rocks // Econ. Geol. Society of Economic Geologists, 2020. Vol. 115, No. 2. P. 279–301.
- 6. *Li P., Boudreau A.E.* Vapor transport of silver and gold in basaltic lava flows // Geology. Geological Society of America, 2019. Vol. 47, No. 9. P. 877–880.
- 7. Symonds R.B., Reed M.H. Calculation of multicomponent chemical equilibria in gas-solid-liquid systems: Calculation methods, thermochemical data, and applications to studies of high-temperature volcanic gases with examples from Mt. St. Helens // Am. J. Sci. States). 1993. Vol. 293, No. 8.
- 8. Sharygin V.V et al. Copper-containing magnesio-ferrite in vesicular trachyandesite in a lava tube from the 2012–2013 eruption of the Tolbachik volcano, Kamchatka, Russia // Minerals. Multidisciplinary Digital Publishing Institute, 2018. Vol. 8, No. 11. P. 514.
- 9. Kamenetsky V.S. et al. High-temperature gold-copper extraction with chloride flux in lava tubes of Tolba-

- chik volcano (Kamchatka) // Terra Nov. Wiley Online Library, 2019. Vol. 31, No. 6. P. 511–517.
- 10. *Ovalle J.T. et al.* Formation of massive iron deposits linked to explosive volcanic eruptions // Sci. Rep. 2018. Vol. 8, No. 1. P. 14855.
- 11. *Kostin A.V.* Immiscible silica- and iron-rich melts at the Kildyam volcano complex (central Yakutia, Russia) // Arct. Subarct. Nat. Resour. 2020. Vol. 25, No. 2. P. 25–44.
- 12. Afanasiev V. P., Pokhilenko N. P., Grinenko V. S., Kostin A. V., Malkovets V. G. O.O.B. Kimberlitic magmatism in the south-western flank of the Vilui basin // Dokl. Earth Sci. 2020. Vol. 2, No. 490. P. 5–9.
- 13. *Smelov A.P., Surnin A.A.* Gold of the city of Yakutsk // Sci. First Hand. 2010. № 4 (34). P. 16–19.
- 14. Kostin A.V., Grinenko V.S., Oleinikov O.B., Jelonkina M.S., Krivoshapkin I.I. V.A.E. The first data about the manifestation of the Upper Cretaceous volcanism of transition zone «Siberian platform Verkhoyansk-Kolyma folded area» // Arct. Subarct. Nat. Resour. 2015. Vol. 1, No. 77. P. 30–36.
- 15. Grinenko V.S., Kostin A.V., Kirichkova A.I. Z.M.S. NEW DATA ON THE UPPER JURASSIC LOWER CRETACEOUS ROCKS IN THE EASTERN SIBERI-AN PLATFORM // Vestn. Vor. Gos. Univ. Ser. Geol. 2018. Vol. 2. P. 48–55.
- 16. Kostin A.V, Trunilina V.A. Volcanogenic creations of Kangalassky terrace (left bank of the Lena River, Central Yakutia) // Adv. Curr. Nat. Sci. 2018. Vol. 5. P. 92–100.
- 17. Bakillah M., Liang S. Open geospatial data, software and standards // Open Geospatial Data, Softw. Stand. 2016. Vol. 1, No. 1. P. 1.
- 18. *Minghini M. et al.* Geospatial openness: from software to standards & data // Open Geospatial Data, Softw. Stand. 2020. Vol. 5, No. 1. P. 1.
- 19. Andersen J.C. Postmagmatic sulphur loss in the Skaergaard intrusion: implications for the formation of the Platinova Reef // Lithos. Elsevier, 2006. Vol. 92, No. 1–2. P. 198–221.
- 20. *Kostin A.V.* A new geological feature of volcanic origin in the Lena-Vilyui watershed (east of Siberian platform) // Adv. Curr. Nat. Sci. 2017. Vol. 2. P. 100–105.
- 21. *Tegner C*. Iron in plagioclase as a monitor of the differentiation of the Skaergaard intrusion // Contrib. to Mineral. Petrol. 1997. Vol. 128, No. 1. P. 45–51.
- 22. Charlier B., Namur O., Grove T.L. Compositional and kinetic controls on liquid immiscibility in ferrobasalt–rhyolite volcanic and plutonic series // Geochim. Cosmochim. Acta. 2013. Vol. 113. P. 79–93.

- 23. *Honour V.C. et al.* Microstructural evolution of silicate immiscible liquids in ferrobasalts // Contrib. to Mineral. Petrol. 2019. Vol. 174, No. 9. P. 77.
- 24. *LEEMAN W.P., VITALIANO C.J.* Petrology of McKinney Basalt, Snake River Plain, Idaho // GSA Bull. 1976. Vol. 87, No. 12. P. 1777–1792.
- 25. *Philpotts A.R.* Compositions of immiscible liquids in volcanic rocks // Contrib. to Mineral. Petrol. Springer, 1982. Vol. 80, № 3. P. 201–218.
- 26. Waitt R.B. Great Holocene Floods along Jökulsá á Fjöllum, North Iceland // Flood and Megaflood Processes and Deposits. 2002. P. 37–51.
- 27. LARSEN G. et al. A shift in eruption mode of Hekla volcano, Iceland, 3000 years ago: two-coloured Hekla tephra series, characteristics, dispersal and age // J. Quat. Sci. John Wiley & Sons, Ltd, 2020. Vol. 35, No. 1–2. P. 143–154.
- 28. Tomshin M.D. et al. Native iron in the dolerites of the Aikhal sill (the first discovery in Yakutia) // Arct. Subarct. Nat. Resour. Государственное учреждение Академия наук Республики Саха (Якутия), 2019. Vol. 24, No. 3. P. 50–63.
- 29. *Horwell C.J. et al.* The nature and formation of cristobalite at the Soufrière Hills volcano, Montserrat: implications for the petrology and stability of silicic lava domes // Bull. Volcanol. Springer, 2013. Vol. 75, No. 3. P. 1–19.
- 30. *Reich M. et al.* Formation of cristobalite nanofibers during explosive volcanic eruptions // Geology. Geological Society of America, 2009. Vol. 37, No. 5. P. 435–438.
- 31. Schipper C.I. et al. Cristobalite in the 2011–2012 Cordón Caulle eruption (Chile) // Bull. Volcanol. 2015. Vol. 77, No. 5. P. 34.
- 32. *Nadeau O*. Ore metals beneath volcanoes // Nat. Geosci. 2015. Vol. 8, No. 3. P. 168–170.
- 33. Silaev V.I. et al. Mineral Phase Paragenesis in Explosive Ejecta Discharged by Recent Eruptions in Kamchatka and on the Kuril Islands. Part 2. Accessory Minerals of the Tolbachik Type Diamonds // J. Volcanol. Seismol. 2019. Vol. 13, No. 6. P. 376–388.
- 34. *Kamenetsky V.S. et al.* Silicate-sulfide liquid immiscibility in modern arc basalt (Tolbachik volcano, Kamchatka): Part II. Composition, liquidus assemblage and fractionation of the silicate melt // Chem. Geol. 2017. Vol. 471. P. 92–110.
- 35. Zelenski M. et al. Silicate-sulfide liquid immiscibility in modern arc basalt (Tolbachik volcano, Kamchatka): Part I. Occurrence and compositions of sulfide melts // Chem. Geol. 2018. Vol. 478. P. 102–111.

MINERALIZATION IN THE KILDYAM MAFIC VOLCANIC ROCKS

36. *Li C., Boudreau A.E.* The origin of high-Cu/S trusion, East Greenland // Geology. GeoScienceWorld, sulfides by shallow-level degassing in the Skaergaard in-

Поступила в редакцию 10.04.2021 Принята к публикации 24.05.2021

About the author

KOSTIN Aleksey Valentinovich, Dr. Sci. (Geology and Mineralogy), chief reseacher, Diamond and Precious Metals Geology Institute SB RAS, 39 Lenina pr., Yakutsk 677000, Russia, http://orcid.org/0000-0002-5778-6505, a.v.kostin2006@rambler.ru

Citation

Kostin A.V. Mineralization in the Kildyam mafic volcanic rocks – a magmatic contribution to ore-forming fluids (Central Yakutia, Russia) // Arctic and Subarctic Natural Resources. 2021. Vol. 26, No. 2. pp. 49–71. (In Russ.) https://doi.org/10.31242/2618-9712-2021-26-2-3